The Effect of an Anisotropic Pressure of Thermal or Energetic Particles on Resistive Wall Mode Stability

J.W. Berkery,[1, a)] R. Betti,[2] S.A. Sabbagh,[1] N. Gorelenkov,[3] L. Guazzotto,[2] J. Manickam,[3] and M. Podestà[3]
[1)] *Department of Applied Physics and Applied Mathematics, Columbia University, New York, New York 10027*
[2)] *Laboratory for Laser Energetics, University of Rochester, Rochester, New York 14623*
[3)] *Princeton Plasma Physics Laboratory, Princeton University, Princeton, New Jersey 08543*

(Dated: 29 February 2012)

The effect of an anisotropic pressure of thermal or energetic particles on resistive wall mode (RWM) stability is derived through kinetic theory and assessed through calculation with the `MISK` code [B. Hu, *et al.*, Phys. Plasmas **12**, 057301 (2005)]. The fluid anisotropy is treated as a small perturbation on the plasma equilibrium, and a complete treatment without a high frequency mode rotation assumption leads to kinetic terms in addition to anisotropy corrections to the fluid terms. Using a perturbed bi-Maxwellian distribution function for thermal particles, with a higher temperature perpendicular to the magnetic field than parallel, the ballooning destabilization term is reduced while the stabilizing kinetic effects of the trapped thermal ions are enhanced, leading to an increase in RWM stability. For energetic particles, the consequences of perpendicular vs. parallel injection and broad vs. narrow spreading in pitch angle of beam ions with an anisotropic slowing-down distribution in the National Spherical Torus Experiment (NSTX) [M. Ono, *et al.*, Nucl. Fusion **40**, 557 (2000)] are considered. The ballooning term is modified to be less destabilizing and together with the kinetic effects, the overall effect of beam ions is to be significantly stabilizing, maximizing at more perpendicular injection and narrow spreading. [DOI: 00.0000/0.0000000]

I. INTRODUCTION

Tokamak fusion plasmas generate energy most efficiently when the ratio of plasma stored energy to magnetic confining field energy (characterized by the quantity β_N) is high. In order to reach these conditions without disruption of the plasma current due to the growth of MHD kink-ballooning modes of instability, these modes must be stabilized. The presence of a resistive wall around the plasma can slow the growth of these modes down to the time scale of penetration of the magnetic perturbations through the wall, converting the mode into a resistive wall mode (RWM). However, the RWM can also disrupt the plasma when β_N is above the so-called no-wall limit unless it is itself stabilized by passive or active means[1].

It has long been recognized that anisotropy of the plasma pressure with respect to the direction of the magnetic field can play a role in plasma stability. Consideration of anisotropy goes back as far as Refs. [2] and [3]; some more recent prominent examples include Refs. [4] and [5]. One possible course of action is to consider the perturbed perpendicular and parallel pressures from Chew-Goldberger-Low (CGL)[6] theory. It will be demonstrated here, however, that using CGL theory is akin to an assumption of a high frequency mode, which is not applicable to the RWM. Instead, kinetic theory, in which the perturbed pressures are rigorously solved from a perturbed distribution function, will be employed. Kinetic theory, recently expanded to be relevant to low frequency modes such as the RWM[7], has been successfully compared to experimental instability[8–10] in the National Spherical Torus Experiment[11] (NSTX) with calculations from the `MISK` code[12]. In particular, the importance of resonances between the plasma rotation and the motions of thermal particles was elucidated. Here we will expand the treatment of those thermal particles to include the possibility of anisotropy, such as might arise when Maxwellian electrons are modified by electron cyclotron current drive (ECCD) or electron cyclotron resonance heating (ECRH)[13]. It was then recognized that energetic particles, such as beam ions, can also be important to RWM stability[10,14–16]. This effect has been studied experimentally, such as a tilted neutral beam injection experiment in DIII-D [?] , and theoretically, as in Ref. [15] which looked at the effect of the deposition location in Ψ and of the beam injection energy. Radially localized anisotropy of ions will not be considered here, but we note that much of the same physics applies, and is important for stabilization of sawteeth (using heating from ICRF[17,18] or NBI[18,19]).

In Sec. II we outline the Energy Principle approach to RWM stability calculations with a perturbative approach. In order to use such an approach we must then demonstrate in Sec. III that anisotropy of the pressure represents a small perturbation on the equilibrium. In Sec. IV an anisotropic perturbed pressure tensor is used to determine a

[a)] Electronic mail: jberkery@pppl.gov

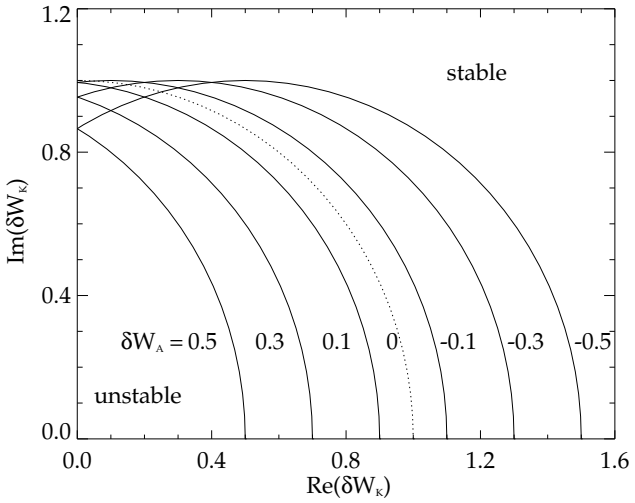

FIG. 1. Example of a stability diagram, showing contours of $\gamma\tau_w = 0$ with $\delta W_\infty = -1$ and $\delta W_b = 1$ in arbitrary units, modified by anisotropy. Positive δW_A shifts the unstable region to the left, while negative δW_A shifts it to the right.

general equation for the anisotropic corrections to the fluid δW term. Equations for the kinetic effects depend on the distribution function of the particles chosen; in Sec. V these are derived for two specific cases: a bi-Maxwellian distribution of thermal particles and an anisotropic slowing-down distribution for energetic particles. In Sec. VI we return to the fluid anisotropic correction specifically for the pressure-driven ballooning destabilization term and incorporate these two distribution functions as well. Calculations with the `MISK` code are carried out using these derived expressions in Sec. VII for an analytical Solov'ev equilibrium to test the effect of thermal particle anisotropy, and a real NSTX experimental equilibrium to test the effect of energetic particle anisotropy and its dependence on injection pitch angle and width of the spreading in pitch angle. Further possible improvements to the energetic particle treatment are discussed in Sec. VIII and finally conclusions are drawn.

II. STABILITY CALCULATION THROUGH AN ENERGY PRINCIPLE APPROACH

Pressure anisotropy leads to a modified Energy Principle expression for the complex mode frequency, ω, normalized by the wall time constant τ_w, where $\omega = \omega_r + i\gamma$ is comprised of the growth rate, γ, and real mode rotation frequency, ω_r:

$$-i\omega\tau_w = -\frac{\delta W_V^\infty + \delta W_F + \delta W_A + \delta W_K}{\delta W_V^b + \delta W_F + \delta W_A + \delta W_K}. \tag{1}$$

Here δW_V^∞ and δW_V^b are the usual changes in vacuum potential energy without a wall and with an ideal wall, respectively. δW_F is the usual isotropic fluid term, while δW_A is an anisotropic fluid correction and δW_K is the kinetic term, which also must be modified by anisotropy. In Ref. [8] stability diagrams were described, which show contours of constant normalized growth rate on plots of $Im(\delta W_K)$ vs. $Re(\delta W_K)$. Now the anisotropy term modifies those diagrams by adding $-\delta W_A$ to the offset a of the $\gamma\tau_w = 0$ curve that defines the unstable region, as shown in the example in Fig. 1.

Now, in order to solve for the δW terms, we use a plasma force balance $\rho(d\mathbf{v}/dt) = \mathbf{j}\times\mathbf{B} - \boldsymbol{\nabla}\cdot\mathbb{P}$, which leads to an expression for the change in potential energy of the plasma due to a small displacement $\boldsymbol{\xi}_\perp$:

$$\delta W = \frac{1}{2}\int \boldsymbol{\xi}_\perp^* \cdot \left[\mathbf{j_0}\times\tilde{\mathbf{B}} + \tilde{\mathbf{j}}\times\mathbf{B_0} - \boldsymbol{\nabla}\cdot\tilde{\mathbb{P}}\right] d\mathbf{V}, \tag{2}$$

where x_0 are equilibrium quantities, $\tilde{x}$ are perturbed quantities, $\mathbf{j}$ is the plasma current, $\mathbf{B}$ is the magnetic field, ρ is the density, $\mathbf{v}$ is the velocity, $\mathbb{P}$ is the pressure tensor, and $\mathbf{V}$ is the plasma volume. In the perturbative approach to stability calculations, it is assumed that the RWM eigenfunction, $\xi_\perp$, is unchanged by both the kinetic effects that

come in through $\tilde{\mathbb{P}}$ and, now, the anisotropy of the equilibrium as well. This is as opposed to the alternative approach in which $\tilde{\mathbb{P}}$, $\xi_\perp$, and ω are self-consistently calculated.

The well known problem of closure of the set of equations now requires us to make specification for the equilibrium and perturbed pressures. First, however, we will examine the effect of anisotropy on the plasma equilibrium to assure the applicability of the perturbative approach to the problem.

III. EQUILIBRIUM

Anisotropy of the plasma pressure can affect the plasma equilibrium[20–26]. In the present work, however, we will use the isotropic equilibrium as a basis for stability calculations. Therefore we must now demonstrate that the anisotropy can be considered to be a small perturbation on the isotropic equilibrium that can be neglected.

The plasma equilibrium relation comes from the force balance of Sec. II with the plasma velocity considered constant, so that $\mathbf{j}\times\mathbf{B} = \boldsymbol{\nabla}\cdot\mathbb{P}$. We will consider a pressure tensor with separate components in the directions parallel and perpendicular to the magnetic field,

$$\mathbb{P} = p_\parallel \hat{\mathbf{b}}\hat{\mathbf{b}} + p_\perp\left(\hat{\mathbf{I}} - \hat{\mathbf{b}}\hat{\mathbf{b}}\right), \tag{3}$$

where $\hat{\mathbf{I}}$ is the identity tensor and $\hat{\mathbf{b}} = \mathbf{B}/B$.

Let us now also define an anisotropy parameter[5,24,27,28]

$$\sigma = 1 + \frac{\mu_0\left(p_\perp - p_\parallel\right)}{B^2}, \tag{4}$$

which we note is unity when $p_\perp = p_\parallel$. It is easy to see that for a given normalized pressure difference $(p_\perp - p_\parallel)/p$, $|\sigma - 1|$ is larger for higher beta plasmas.

Then using Ampere's law and the anisotropic pressure tensor from Eq. 3, we have:

$$\frac{1}{\mu_0}\left(\boldsymbol{\nabla}\times\mathbf{B}\right)\times\mathbf{B} = \boldsymbol{\nabla}\cdot\left(p_\parallel\hat{\mathbf{b}}\hat{\mathbf{b}} + p_\perp\left(\hat{\mathbf{I}} - \hat{\mathbf{b}}\hat{\mathbf{b}}\right)\right). \tag{5}$$

Now using the magnetic curvature, $\boldsymbol{\kappa} = \hat{\mathbf{b}}\cdot\boldsymbol{\nabla}\hat{\mathbf{b}}$, and

$$\boldsymbol{\nabla}\cdot\left(\hat{\mathbf{b}}\hat{\mathbf{b}}\right) = \hat{\mathbf{b}}\nabla_\parallel + \boldsymbol{\kappa} + \hat{\mathbf{b}}\left(\boldsymbol{\nabla}\cdot\hat{\mathbf{b}}\right), \tag{6}$$

$$\boldsymbol{\nabla}\cdot\left(\hat{\mathbf{I}} - \hat{\mathbf{b}}\hat{\mathbf{b}}\right) = \boldsymbol{\nabla}_\perp - \boldsymbol{\kappa} - \hat{\mathbf{b}}\left(\boldsymbol{\nabla}\cdot\hat{\mathbf{b}}\right), \tag{7}$$

we have

$$-\boldsymbol{\nabla}\frac{\mathbf{B}^2}{2\mu_0} + \left(\boldsymbol{\kappa} + \hat{\mathbf{b}}\left(\boldsymbol{\nabla}\cdot\hat{\mathbf{b}}\right)\right)\frac{B^2}{\mu_0} = \boldsymbol{\nabla}_\perp p_\perp + \hat{\mathbf{b}}\nabla_\parallel p_\parallel + \left(\boldsymbol{\kappa} + \hat{\mathbf{b}}\left(\boldsymbol{\nabla}\cdot\hat{\mathbf{b}}\right)\right)\left(p_\parallel - p_\perp\right). \tag{8}$$

In the perpendicular direction, the equilibrium is[5]

$$\boldsymbol{\nabla}_\perp\left(\frac{\mathbf{B}^2}{2\mu_0} + \frac{p_\parallel + p_\perp}{2\sigma}\right) = \boldsymbol{\kappa}\frac{B^2}{\mu_0}, \tag{9}$$

In the isotropic case, the equilibrium relation reduces to $\boldsymbol{\nabla}_\perp\left(\frac{\mathbf{B}^2}{2\mu_0} + p\right) = \boldsymbol{\kappa}\frac{B^2}{\mu_0}$. The equilibrium relation in the anisotropic equilibrium pressure case can be written in this same form, if we define a new quantity which is like a corrected magnetic field $\mathbf{D} = \mathbf{B}\sqrt{\sigma}$, so that,

$$\boldsymbol{\nabla}_\perp\left(\frac{\mathbf{D}^2}{2\mu_0} + p_{\text{avg}}\right) = \boldsymbol{\kappa}\frac{D^2}{\mu_0}, \tag{10}$$

where we have defined $p_{\text{avg}} = (p_\parallel + p_\perp)/2$. This is useful because it means that the plasma equilibrium can be considered to first order the isotropic equilibrium, and then having an anisotropic correction of the second order. As long as σ is not much different from unity, we will consider the perturbative approach to the problem to be valid.

IV. THE ANISOTROPIC PERTURBED PRESSURE TENSOR

One must now be careful in linearizing Eq. 3 for obtaining $\tilde{\mathbb{P}}$ for use in Eq. 2, remembering that $\hat{\mathbf{b}}$ can also be perturbed[5]. Therefore,

$$\tilde{\mathbb{P}} = \tilde{p}_{\parallel}\hat{\mathbf{b}}\hat{\mathbf{b}} + \tilde{p}_{\perp}\left(\hat{\mathbf{I}} - \hat{\mathbf{b}}\hat{\mathbf{b}}\right) + (p_{\parallel} - p_{\perp})B^{-2}\left(\tilde{\mathbf{B}}\mathbf{B} + \mathbf{B}\tilde{\mathbf{B}}\right). \tag{11}$$

At this point the problem naturally separates into fluid and kinetic approaches. In the fluid approach the perturbed pressures are given in terms of macroscopic quantities. There are two common fluid approximations. The first is to assume the equilibrium pressure and the perturbed pressure are isotropic so, $\boldsymbol{\nabla}\cdot\tilde{\mathbb{P}} = \nabla\tilde{p}$, which results in a fluid compressibility term, $\frac{1}{2}\int \gamma p|\boldsymbol{\nabla}\cdot\boldsymbol{\xi}_{\perp}|^2 d\mathbf{V}$. Then the adiabatic equation is used to find $\tilde{p}$. In the second common fluid approach, two adiabatic equations are used to find the two Chew-Golberger-Low (CGL)[6] perturbed pressures, $\tilde{p}_{\perp}$ and $\tilde{p}_{\parallel}$. This method is outlined in appendix B, and could result in the calculation of a δW_{CGL} term[29,30].

In the kinetic approach[5,31–34], $\tilde{p}_{\perp}$ and $\tilde{p}_{\parallel}$ are defined by using the perturbed distribution function $\tilde{f}$. First, we write:

$$\tilde{\mathbb{P}} = \sum_j m_j \int \mathbf{v}\mathbf{v}\left(\tilde{f}_j + \frac{\partial f_j}{\partial B}\boldsymbol{\xi}_{\perp}\cdot\boldsymbol{\nabla}\mathbf{B} + \frac{\partial f_j}{\partial \Phi}\boldsymbol{\xi}_{\perp}\cdot\boldsymbol{\nabla}\boldsymbol{\Phi}\right) d^3\mathbf{v}, \tag{12}$$

and then use for $\tilde{f}_j$:

$$\tilde{f}_j = -\boldsymbol{\xi}_{\perp}\cdot\boldsymbol{\nabla}f_j + Z_j e\frac{\partial f_j}{\partial \varepsilon}\tilde{\boldsymbol{\Phi}} + im_j\left(\omega\frac{\partial f_j}{\partial \varepsilon} - n\frac{\partial f_j}{\partial P_{\phi}}\right)(\mathbf{v}\cdot\boldsymbol{\xi}_{\perp} - \tilde{s}_j) - \frac{m_j}{B}\frac{\partial f_j}{\partial \mu}\left(-i\omega\boldsymbol{\xi}_{\perp}\cdot\mathbf{v}_{\perp} + \frac{\mu}{m_j}\tilde{\mathbf{B}}_{\parallel} + \frac{v_{\parallel}}{B}\mathbf{v}_{\perp}\cdot\tilde{\mathbf{B}}\right). \tag{13}$$

Here $\boldsymbol{\Phi}$ is the potential, P_{ϕ} is the toroidal canonical momentum, n is the toroidal mode number, and μ is the magnetic moment. The quantitiy $\tilde{s}_j$ represents the integral along the unperturbed orbits and is essentially the term that gives rise to kinetic effects in the problem (see for example Ref.[30]).

Generally it is assumed that the equilibrium pressure is isotropic ($p_{\parallel} = p_{\perp}$), even in the kinetic approach. Here we extend that approach so that in Eq. 11 the final term (perturbation of the direction of the magnetic field in an anisotropic equilibrium pressure plasma[5]) is not zero, and $\partial f_j/\partial B$ is also not zero in Eq. 12. Rather, one can show that[23,25] $p_{\parallel} - p_{\perp} = B(\partial p_{\parallel}/\partial B)$. After carrying through much algebra, and defining $\tilde{\boldsymbol{\mathcal{Z}}} = Z_j e\left(\tilde{\boldsymbol{\Phi}} + \boldsymbol{\xi}_{\perp}\cdot\boldsymbol{\nabla}\Phi_0\right)$, we arrive at the expression

$$\begin{aligned}\tilde{\mathbb{P}} =& \hat{\mathbf{b}}\hat{\mathbf{b}}\left[-\boldsymbol{\xi}_{\perp}\cdot\boldsymbol{\nabla}p_{\parallel} - (\boldsymbol{\nabla}\cdot\boldsymbol{\xi}_{\perp} + \boldsymbol{\kappa}\cdot\boldsymbol{\xi}_{\perp})B\frac{\partial p_{\parallel}}{\partial B} + \sum_j m_j\int v_{\parallel}^2\left[im_j\left(\omega\frac{\partial f_j}{\partial \varepsilon} - n\frac{\partial f_j}{\partial P_{\phi}}\right)\tilde{s}_j + \tilde{\boldsymbol{\mathcal{Z}}}\frac{\partial f_j}{\partial \varepsilon}\right]d^3\mathbf{v}\right] \qquad (14)\\ &+ \left(\hat{\mathbf{I}} - \hat{\mathbf{b}}\hat{\mathbf{b}}\right)\left[-\boldsymbol{\xi}_{\perp}\cdot\boldsymbol{\nabla}p_{\perp} - (\boldsymbol{\nabla}\cdot\boldsymbol{\xi}_{\perp} + \boldsymbol{\kappa}\cdot\boldsymbol{\xi}_{\perp})B\frac{\partial p_{\perp}}{\partial B} + \sum_j m_j\int \frac{1}{2}v_{\perp}^2\left[im_j\left(\omega\frac{\partial f_j}{\partial \varepsilon} - n\frac{\partial f_j}{\partial P_{\phi}}\right)\tilde{s}_j + \tilde{\boldsymbol{\mathcal{Z}}}\frac{\partial f_j}{\partial \varepsilon}\right]d^3\mathbf{v}\right]\\ &+ \frac{1}{B}\left(\hat{\mathbf{b}}\tilde{\mathbf{B}}_{\perp} + \tilde{\mathbf{B}}_{\perp}\hat{\mathbf{b}}\right)(p_{\parallel} - p_{\perp}). \qquad (15)\end{aligned}$$

Finally, this represents a form of the perturbed pressure tensor that we can use to evaluate δW, from Eq. 2.

It is useful when doing so to separate out the various modes of instability, for example Eq. (39) in Ref. [35], or Eq. (58) in Ref. [5]. Then the various terms of the potential energy can be seen to be contributions from stabilizing shear Alfvén waves, fast magneto-acoustic (compressional Alfvén) waves, and the two terms that can drive instability by current driven kink or pressure driven ballooning modes. Finally, using an alternative form for $\mathbf{j_0}\times\tilde{\mathbf{B}} + \tilde{\mathbf{j}}\times\mathbf{B_0}$, $\boldsymbol{\xi}_{\perp}^*\cdot\boldsymbol{\nabla}\cdot\hat{\mathbf{b}}\hat{\mathbf{b}} = \boldsymbol{\kappa}\cdot\boldsymbol{\xi}_{\perp}^*$, and $\boldsymbol{\xi}_{\perp}^*\cdot\boldsymbol{\nabla}\cdot(\hat{\mathbf{I}} - \hat{\mathbf{b}}\hat{\mathbf{b}}) = -(\boldsymbol{\nabla}\cdot\boldsymbol{\xi}_{\perp}^* + \boldsymbol{\kappa}\cdot\boldsymbol{\xi}_{\perp}^*)$ from Eqs. 6 and 7, a fair bit of algebraic manipulation, and splitting δW into isotropic fluid, anisotropic fluid, and kinetic plus electrostatic parts, we have

$$\delta W_F = \frac{1}{2}\int\Bigg\{ \underbrace{\left(-\frac{|\tilde{\boldsymbol{B}}_\perp|^2}{\mu_0}\right)}_{\text{shearAlfvén}} \underbrace{-\frac{B^2}{\mu_0}|\boldsymbol{\nabla}\cdot\boldsymbol{\xi}_\perp + 2\boldsymbol{\xi}_\perp\cdot\boldsymbol{\kappa}|^2}_{\text{fast magneto-acoustic}} \underbrace{+ j_\parallel\left(\boldsymbol{\xi}_\perp^*\times\hat{\boldsymbol{b}}\right)\cdot\tilde{\boldsymbol{B}}_\perp}_{\text{kink}} \Bigg) \underbrace{+2\left(\boldsymbol{\kappa}\cdot\boldsymbol{\xi}_\perp^*\right)\left(\boldsymbol{\xi}_\perp\cdot\boldsymbol{\nabla}p_{\text{avg}}\right)}_{\text{ballooning}} \Bigg\} d\mathbf{V}, \tag{16}$$

$$\delta W_A = \frac{1}{2}\int\left\{(\sigma-1)\left(-\frac{|\tilde{\boldsymbol{B}}_\perp|^2}{\mu_0} - \frac{B^2}{\mu_0}|\boldsymbol{\nabla}\cdot\boldsymbol{\xi}_\perp + 2\boldsymbol{\xi}_\perp\cdot\boldsymbol{\kappa}|^2 + j_\parallel\left(\boldsymbol{\xi}_\perp^*\times\hat{\boldsymbol{b}}\right)\cdot\tilde{\boldsymbol{B}}_\perp\right) - 2B\left|\boldsymbol{\nabla}\cdot\boldsymbol{\xi}_\perp + \boldsymbol{\kappa}\cdot\boldsymbol{\xi}_\perp\right|^2\frac{\partial p_{\text{avg}}}{\partial B}\right\} d\mathbf{V}, \tag{17}$$

and

$$\delta W_{K+\Phi} = \frac{1}{2}\sum_j\int\int\frac{1}{2}m_j v^2\left(\frac{v_\perp^2}{v^2}\boldsymbol{\nabla}\cdot\boldsymbol{\xi}_\perp^* + \left(\frac{v_\perp^2}{v^2} - 2\frac{v_\parallel^2}{v^2}\right)\boldsymbol{\kappa}\cdot\boldsymbol{\xi}_\perp^*\right)\left[im_j\left(\omega\frac{\partial f_j}{\partial\varepsilon} - n\frac{\partial f_j}{\partial P_\phi}\right)\tilde{s}_j + \tilde{\boldsymbol{\mathcal{Z}}}\frac{\partial f_j}{\partial\varepsilon}\right] d^3\mathbf{v}d\mathbf{V}. \tag{18}$$

Similar results have been previously derived in, for example, Refs. [4, 36–38]. One can easily see that if the equilibrium pressure is isotropic, δW_A is zero.

The above equation for δW_F is solved by various numerical codes (with $p_{\text{avg}} = p$, a flux function). For example, the `PEST` code[39] solves for δW_F, in the form of Eq. (17) of Ref. [40], and uses the `VACUUM` code[41] to solve for δW_V. In the following we will consider $p_{\text{avg}} \approx p$ in Eq. 16 so that δW_F can be considered unchanged from the isotropic case. The correction due to anisotropy will come entirely from the δW_A term. Note that the $\sigma - 1$ correction to the shear Alfvén, magnetic compression, and kink destabilization terms will necessarily be small due to the restriction of $\sigma \ll 1$ imposed by equilibrium considerations in Sec. III.

The last term of Eq. 17 represents a modification of the pressure-driven ballooning destabilization term, which we will call δW_{A2}. This term has a different anisotropy correction than the others because of its explicit dependence on the pressure. It will be separately, and rigorously, calculated and discussed further in Sec. VI.

The fluid terms ($\delta W_F + \delta W_A$) should be self-adjoint and therefore strictly real[42]. In particular, δW_{A2} in Eq. 17 is obviously self-adjoint, as are the first two terms (the shear Alfvén and the magnetic compression terms) of δW_A in Eq. 17 and δW_F in Eq. 16. When the equilibrium pressure is isotropic ($\sigma = 1$ and $p_{\text{avg}} = p$), one can show that the last two terms of δW_F (the kink and ballooning destabilization terms) are as well. With anisotropy that property is no longer obvious, but a lengthly manipulation can be used to show that indeed $\delta W_F + \delta W_A$ is still self-adjoint (see appendix C).

Finally, $\delta W_{K+\Phi}$ represents the kinetic plus electrostatic terms. In the following, we will drop the electrostatic contribution and only consider the kinetic term, with the distribution function f_j being for anisotropic particles.

V. KINETIC EFFECTS WITH ANISOTROPIC PRESSURE

An expression for δW_K that shows explicitly the dependence on the distribution function of the particles considered can be derived from Eq. 18 (ignoring electrostatic effects) and written[10,15]:

$$\delta W_K = \sum_j\sum_{l=-\infty}^{\infty} 2\sqrt{2}\pi^2\int\int\int\left[\left|\langle HT_j\rangle\right|^2\lambda_{j,l}\frac{f_j}{T_j}\right]\frac{\hat{\tau}}{m_j^{\frac{3}{2}}B}|\chi|\varepsilon^{\frac{1}{2}}d\varepsilon d\chi d\Psi. \tag{19}$$

Here j denotes the particle type that is being considered (ions or electrons), ε is energy, $\chi = v_\parallel/v$ is the pitch angle, Ψ is the magnetic flux, H and $\hat{\tau}$ are given by Eqs. (12) and (13) of Ref. [43], and we have defined the frequency resonance fraction, $\lambda_{j,l}$, as:

$$\lambda_{j,l} = \frac{\frac{T_j}{f_j}\left(\left(\omega - n\omega_E\right)\frac{\partial f_j}{\partial\varepsilon} - \frac{n}{Z_j e}\frac{\partial f_j}{\partial\Psi}\right)}{n\langle\omega_D^j\rangle + \left(l + \alpha nq\right)\omega_b^j - i\nu_{\text{eff}}^j + n\omega_E - \omega}. \tag{20}$$

Here ω_E is the $E \times B$ frequency, $\langle \omega_D \rangle$ is the bounce-averaged precession drift frequency, l is the bounce harmonic, $\alpha = 0$ for trapped particles or $\alpha = 1$ for circulating particles, ω_b is the bounce frequency, and ν_{eff} is the effective collision frequency. Note that T_j is a dummy variable that cancels out in the end.

Clearly the kinetic effects depend on the particle distribution function through its derivatives with respect to Ψ and energy[10,15]. We will see in the next section that the derivative $\partial f_j/\partial \chi$ enters into the fluid anisotropy term as well.

A. Thermal Particles: bi-Maxwellian Distribution

In order to be consistent with the assumption of different pressures in the parallel and perpendicular directions, one should use a bi-Maxwellian distribution, which has pressure anisotropy due to different temperatures parallel and perpendicular to the magnetic field, in δW_K. The Maxwellian distribution is really just a special case of the more general bi-Maxwellian, with $T_{j\parallel} = T_{j\perp}$, so the bi-Maxwellian form can be used in general.

$$f_j^{bM}(\varepsilon, \Psi, \chi) = n_j \left(\frac{m_j}{2\pi}\right)^{\frac{3}{2}} \frac{1}{T_{j\perp} T_{j\parallel}^{\frac{1}{2}}} e^{-\varepsilon\chi^2/T_{j\parallel}} e^{-\varepsilon(1-\chi^2)/T_{j\perp}}. \tag{21}$$

Here j denotes the particle type that is being considered (ions or electrons) and bM indicates bi-Maxwellian, ε is energy, $\chi = v_\parallel/v$ is the pitch angle, and Ψ is the magnetic flux. The density, $n_j(\Psi)$, and the two temperatures, $T_{j\parallel}(\Psi)$ and $T_{j\perp}(\Psi)$, are each assumed to be flux functions, so that the two pressures $p_\parallel$ and $p_\perp$ are as well. The pressures are given by $p_\parallel = \sum_j \int m_j v_\parallel^2 f_j d^3\mathbf{v} = \sum_j n_j T_{j\parallel}$ and $p_\perp = \sum_j \int \frac{1}{2} m_j v_\perp^2 f_j d^3\mathbf{v} = \sum_j n_j T_{j\perp}$. One can, of course, recover the Maxwellian, isotropic solution when $T_{j\parallel} = T_{j\perp}$.

We can see from Eq. 21 that

$$\frac{\partial f_j^{bM}}{\partial \varepsilon} = -\frac{f_j^{bM}}{T_j}\left(\frac{T_j}{T_{j\parallel}}\right), \tag{22}$$

and $\partial f_j/\partial \Psi$ takes the form:

$$\frac{\partial f_j^{bM}}{\partial \Psi} = -\frac{f_j^{bM}}{T_j}\left(-\frac{T_j}{n_j}\frac{dn_j}{d\Psi} - \left(\varepsilon\chi^2\frac{T_j}{T_{j\parallel}^2} - \frac{1}{2}\frac{T_j}{T_{j\parallel}}\right)\frac{dT_{j\parallel}}{d\Psi} - \left(\varepsilon(1-\chi^2)\frac{T_j}{T_{j\perp}^2} - \frac{T_j}{T_{j\perp}}\right)\frac{dT_{j\perp}}{d\Psi}\right), \tag{23}$$

Defining $\omega^j_{*T_\parallel} = -(1/Z_j e)(dT_{j\parallel}/d\Psi)$, and $\omega^j_{*T_\perp} = -(1/Z_j e)(dT_{j\perp}/d\Psi)$, then from Eqs. 19 and 20 we find:

$$\delta W_K^{bM} = \sum_j \sum_{l=-\infty}^{\infty} \sqrt{\pi} \int\int\int n_j \left(\frac{1}{T_{j\perp} T_{j\parallel}^{\frac{1}{2}}}\right) \frac{\hat{\tau}}{B} |\chi| \varepsilon^{\frac{5}{2}} e^{-\varepsilon\chi^2/T_{j\parallel}} e^{-\varepsilon(1-\chi)^2/T_{j\perp}} d\varepsilon d\chi d\Psi$$
$$\left[|\langle HT_j/\varepsilon \rangle|^2 \ \frac{n\left(\frac{1}{n_j}\frac{dn_j}{d\Psi} + \left(\varepsilon\chi^2\frac{1}{T_{j\parallel}} - \frac{1}{2}\right)\left(\frac{1}{T_{j\parallel}}\right)\omega^j_{*T_\parallel} + \left(\varepsilon(1-\chi^2)\frac{1}{T_{j\perp}} - 1\right)\left(\frac{1}{T_{j\perp}}\right)\omega^j_{*T_\perp} + \left(\frac{1}{T_{j\parallel}}\right)\omega_E\right) - \left(\frac{1}{T_{j\parallel}}\right)\omega}{n\langle\omega_D^j\rangle + l\omega_b^j - i\nu_{\text{eff}}^j + n\omega_E - \omega} \right]. \tag{24}$$

One can see that when $T_{j\parallel} = T_{j\perp} = T_j$, this equation reduces to the usual form for Maxwellian particles, since the exponential terms together become $e^{-\varepsilon/T_j}$, and the ω_{*T} terms become $(\varepsilon/T_j - \frac{3}{2})\omega_{*T}$.

Additionally one could, if desired, derive an expression for the kinetic term under the CGL perturbed pressure assumptions by taking the limit of $\omega \to \infty$, although this is no longer applicable to the RWM. One can show that under this high frequency limit, the CGL perturbed pressures are recovered (see appendix B).

B. Energetic Particles: Anisotropic Slowing-down Distribution

Energetic particles can also cause anisotropy of the equilibrium pressure and can be quite important for stability problems[10,14–16,44–48]. The kinetic effects on RWM stability of anisotropic energetic particles was previously considered

in Ref. [10], albeit for a simple example of a slowing-down distribution, and for trapped particles only. Here we extend that analysis to include circulating particles, and to use a more realistic description of the distribution for beam ions. For beam ions, a representative distribution is a slowing-down distribution function[10,49] with a Gaussian distribution of particles in χ,[50] so that

$$f_j^b(\varepsilon,\Psi,\chi) = n_j A_b \left(\frac{m_j}{\varepsilon_b}\right)^{\frac{3}{2}} \frac{1}{\hat{\varepsilon}^{\frac{3}{2}}+\hat{\varepsilon}_c^{\frac{3}{2}}} \frac{1}{\delta\chi} \left(\exp\left[\frac{-(\chi-\chi_0)^2}{\delta\chi^2}\right] + \exp\left[\frac{-(\chi+2+\chi_0)^2}{\delta\chi^2}\right] + \exp\left[\frac{-(\chi-2+\chi_0)^2}{\delta\chi^2}\right]\right). \tag{25}$$

Here $\hat{\varepsilon} = \varepsilon/\varepsilon_b$, where ε_b is the beam injection energy. Note that the subscript j could potentially refer to ions, electrons, or alpha particles, but in the present work we will only consider ions; indeed the superscript b on f_j^b refers to "beam" ions. The additional two exponential terms are included here in order to satisfy the boundary conditions of no diffusive flux[50] at $\chi = -1$ or 1. Here, however, we do not require any conditions on the trapped/circulating boundaries, or symmetry about $\chi = 0$.

The critical energy between slowing down on electrons ($\varepsilon > \varepsilon_c$) vs. slowing down on ions ($\varepsilon < \varepsilon_c$) is[51,52]:

$$\varepsilon_c = \left(\frac{3\sqrt{\pi}}{4}\right)^{\frac{2}{3}} \left(\frac{m_j}{m_e}\right) \left(\frac{m_e}{n_e}\sum_i \left(\frac{n_i Z_i^2}{m_i}\right)\right)^{\frac{2}{3}} T_e. \tag{26}$$

Note that in a deuterium plasma with $n_i = n_e$, $\varepsilon_c/T_e = 18.65(m_j/m_i)$ so that for alpha particles $\hat{\varepsilon}_c \approx 0.01\ T_e$ [keV]. For alpha particles, then, $\hat{\varepsilon}_c \ll 1$ for plasmas with $T_e \ll 100$ keV, so $\hat{\varepsilon}_c = \varepsilon_c/\varepsilon_b$ is quite small in Eq. 25 compared to the range of $0 \le \hat{\varepsilon} \le 1$. For deuterium beam ions $\hat{\varepsilon}_c \approx 0.2\ T_e$ [keV], so $\hat{\varepsilon}_c$ and $\hat{\varepsilon}$ are comparable for plasmas with $T_e \approx 1-10$ keV.

The form of f_j^b above is dependent upon a central pitch angle $\chi_0(\Psi)$, and width $\delta\chi(\varepsilon,\Psi)$. The center of the Gaussian is determined geometrically, by the intersection of the beam line with the magnetic field lines of the particular surfaces, and is therefore, ostensibly, a known quantity. Note that for the general case of non-perpendicular injection, $\chi_0 \neq 0$ and the distribution is not symmetric and therefore the recasting of the formulation of the problem in terms of χ rather than Λ in Ref. [10], Sec. III was indeed necessary.

The spread of the Gaussian depends on the energy of the particles, because the broadening is determined by Coulomb scattering[50]. The form of the Gaussian width is given by[50,53,54]:

$$\delta\chi(\hat{\varepsilon},\Psi) = \sqrt{\delta\chi_0^2(\Psi) - \frac{1}{3}\ln\left[1+\hat{\varepsilon}_c^{\frac{3}{2}}(\Psi)\right] - \frac{1}{3}\ln\left[\frac{\hat{\varepsilon}^{\frac{3}{2}}}{\hat{\varepsilon}^{\frac{3}{2}}+\hat{\varepsilon}_c^{\frac{3}{2}}(\Psi)}\right]}. \tag{27}$$

Here it is implicitly assumed that the energetic particles have the same mass as the thermal ions they are slowing down on (I think). A similar form for $\delta\chi$ is given in Ref. [55].

If we now solve for A_b in terms of the other quantities, then the unknowns that must be specified to fully describe the energetic particle distribution function are $\chi_0(\Psi)$, $\delta\chi_0(\Psi)$, $n_j(\Psi)$, and ε_b. A_b can be found by using $n_j = \int f_j^b d^3\mathbf{v}$, which assures that the energetic particle density profile remains constant regardless of the choice of χ_0 and $\delta\chi_0$, resulting in

$$A_b(\Psi) = \left[4\sqrt{2}\pi \int_0^1 \frac{\hat{\varepsilon}^{\frac{1}{2}}}{\hat{\varepsilon}^{\frac{3}{2}}+\hat{\varepsilon}_c^{\frac{3}{2}}} \frac{\sqrt{\pi}}{4}\left[\mathrm{erf}\left(\frac{\chi_0+3}{\delta\chi}\right) - \mathrm{erf}\left(\frac{\chi_0-3}{\delta\chi}\right)\right] d\hat{\varepsilon}\right]^{-1}. \tag{28}$$

Here we note the difference between the above expression and the equivalent one in Ref. [49] because of the energy dependence of $\delta\chi$ (and similarly for the factor that arises when solving for p_j from f_j^b).

Now that the distribution function is defined, we can use $\partial f_j/\partial\varepsilon$ and $\partial f_j/\partial\Psi$ in Eq. 20. Using

$$\frac{d\delta\chi}{d\hat{\varepsilon}} = -\frac{1}{4}\frac{1}{\delta\chi}\frac{1}{\hat{\varepsilon}}\left(\frac{\hat{\varepsilon}_c^{\frac{3}{2}}}{\hat{\varepsilon}^{\frac{3}{2}}+\hat{\varepsilon}_c^{\frac{3}{2}}}\right), \tag{29}$$

we have

$$\frac{\partial f_j^b}{\partial \varepsilon} = f_j^b \frac{1}{\varepsilon_b}\left[-\frac{3}{2}\frac{\hat{\varepsilon}^{\frac{1}{2}}}{\hat{\varepsilon}^{\frac{3}{2}}+\hat{\varepsilon}_c^{\frac{3}{2}}} + \frac{1}{4}\frac{1}{\delta\chi^2}\frac{1}{\hat{\varepsilon}}\left(\frac{\hat{\varepsilon}_c^{\frac{3}{2}}}{\hat{\varepsilon}^{\frac{3}{2}}+\hat{\varepsilon}_c^{\frac{3}{2}}}\right)\right.$$
$$\left.\left(1-\frac{2}{\delta\chi^2}\frac{(\chi-\chi_0)^2 e^{-(\chi-\chi_0)^2/\delta\chi^2}+(\chi+2+\chi_0)^2 e^{-(\chi+2+\chi_0)^2/\delta\chi^2}+(\chi-2+\chi_0)^2 e^{-(\chi-2+\chi_0)^2/\delta\chi^2}}{e^{-(\chi-\chi_0)^2/\delta\chi^2}+e^{-(\chi+2+\chi_0)^2/\delta\chi^2}+e^{-(\chi-2+\chi_0)^2/\delta\chi^2}}\right)\right]. \quad (30)$$

Note that when $d\delta\chi/d\hat{\varepsilon}=0$, as was previously used in Ref. [10], this expression is considerably simpler.

Similarly, due to the additional dependence of χ_0 and $\delta\chi_0$ on Ψ (and of $\hat{\varepsilon}_c$ on Ψ in the $\delta\chi$ term), $\partial f_j/\partial\Psi$ is given by the complex expression:

$$\frac{\partial f_j^b}{\partial \Psi} = f_j^b\left[\frac{1}{n_j}\frac{dn_j}{d\Psi}+\frac{1}{A_b}\frac{dA_b}{d\Psi}-\frac{1}{\hat{\varepsilon}^{\frac{3}{2}}+\hat{\varepsilon}_c^{\frac{3}{2}}}\frac{d\hat{\varepsilon}_c^{\frac{3}{2}}}{d\Psi}+\frac{1}{e^{-(\chi-\chi_0)^2/\delta\chi^2}+e^{-(\chi+2+\chi_0)^2/\delta\chi^2}+e^{-(\chi-2+\chi_0)^2/\delta\chi^2}}\frac{1}{\delta\chi^2}\right.$$
$$\left(e^{-(\chi-\chi_0)^2/\delta\chi^2}\left(\left(\frac{2(\chi-\chi_0)^2}{\delta\chi^2}-1\right)\frac{\partial\delta\chi}{\partial\Psi}+2(\chi-\chi_0)\frac{d\chi_0}{d\Psi}\right)+\right.$$
$$e^{-(\chi+2+\chi_0)^2/\delta\chi^2}\left(\left(\frac{2(\chi+2+\chi_0)^2}{\delta\chi^2}-1\right)\frac{\partial\delta\chi}{\partial\Psi}-2(\chi+2+\chi_0)\frac{d\chi_0}{d\Psi}\right)+$$
$$\left.\left.e^{-(\chi-2+\chi_0)^2/\delta\chi^2}\left(\left(\frac{2(\chi-2+\chi_0)^2}{\delta\chi^2}-1\right)\frac{\partial\delta\chi}{\partial\Psi}-2(\chi-2+\chi_0)\frac{d\chi_0}{d\Psi}\right)\right)\right], \quad (31)$$

where

$$\frac{\partial\delta\chi}{\partial\Psi}=\frac{1}{\delta\chi}\left[\delta\chi_0\frac{d\delta\chi_0}{d\Psi}+\frac{1}{6}\frac{d\hat{\varepsilon}_c^{\frac{3}{2}}}{d\Psi}\left(\frac{1}{\hat{\varepsilon}^{\frac{3}{2}}+\hat{\varepsilon}_c^{\frac{3}{2}}}-\frac{1}{1+\hat{\varepsilon}_c^{\frac{3}{2}}}\right)\right]. \quad (32)$$

Note that when $d\chi_0/d\Psi=0$ and $d\delta\chi/d\Psi=0$, the above equation reduces to only the first three terms, which is what was previously used in Ref. [10].

The expression for δW_K^b then results from substituting $\partial f_j^b/\partial\varepsilon$ and $\partial f_j^b/\partial\Psi$ into Eq. 20. Of course one can easily recover the isotropic result from Ref. [10] if $\chi_0=0$ and $\delta\chi_0\to\infty$. This is useful, for example, if one wishes to use this anisotropic form generally, but revert to the isotropic form in certain cases, such as for alpha particles.

VI. ANISOTROPIC MODIFICATION OF THE PRESSURE-DRIVEN BALLOONING DESTABILIZATION TERM

Let us return specifically to the final term in Eq. 17 which is like an anisotropic modification to the pressure-driven ballooning destabilization term. Though this is a fluid term, and is strictly real, it can be evaluated in a similar way to the above method for δW_K.

$$\delta W_{A2} = \frac{1}{2}\int\mu\frac{\partial}{\partial\mu}\int\left(m_j v_\parallel^2+\frac{1}{2}m_j v_\perp^2\right)f_j d^3\mathbf{v}|\boldsymbol{\nabla}\cdot\boldsymbol{\xi}_\perp+\boldsymbol{\kappa}\cdot\boldsymbol{\xi}_\perp|^2 d\mathbf{V} \quad (33)$$
$$= \sqrt{2}\pi^2\int\int\int\frac{1}{m_j^{\frac{3}{2}}}|\boldsymbol{\nabla}\cdot\boldsymbol{\xi}_\perp+\boldsymbol{\kappa}\cdot\boldsymbol{\xi}_\perp|^2\left(\chi^4-1\right)\frac{\partial f_j}{\partial\chi}\frac{\hat{\tau}}{B}\varepsilon^{\frac{3}{2}}d\varepsilon d\chi d\boldsymbol{\Psi}. \quad (34)$$

For isotropic particles this term is zero because $\partial f_j/\partial\chi=0$.

A. Thermal Particles: bi-Maxwellian Distribution

In the bi-Maxwellian case $\partial f_j/\partial\chi\neq 0$, but rather,

$$\frac{\partial f_j^{bM}}{\partial \chi} = - f_j^{bM} \left(2\varepsilon|\chi|\right) \left(\frac{1}{T_{j\parallel}} - \frac{1}{T_{j\perp}}\right), \tag{35}$$

so

$$\delta W_{A2}^{bM} = -\sqrt{\pi} \int\int\int n_j \frac{1}{T_{j\perp} T_{j\parallel}^{\frac{1}{2}}} \left(\frac{1}{T_{j_\parallel}} - \frac{1}{T_{j\perp}}\right) \left|\boldsymbol{\nabla}\cdot\boldsymbol{\xi}_\perp + \boldsymbol{\kappa}\cdot\boldsymbol{\xi}_\perp\right|^2 \left(\chi^4 - 1\right) |\chi| e^{-\varepsilon\chi^2/T_{j\parallel}} e^{-\varepsilon(1-\chi^2)/T_{j\perp}} \varepsilon^{\frac{5}{2}} d\varepsilon d\chi d\Psi. \tag{36}$$

The δW_{A2} term does not involve a frequency resonance fraction with various energy dependent terms in the same way that δW_K does. Therefore we can simply perform the energy integration, using[56]: $\int_0^\infty x^{\frac{5}{2}} e^{-ax} dx = (15/8)\sqrt{\pi} a^{-\frac{7}{2}}$, for $a > 0$. Then we have:

$$\delta W_{A2}^{bM} = \frac{15\pi}{8} \int\int n_j \frac{1 - \frac{T_{j\parallel}}{T_{j\perp}}}{T_{j\perp} T_{j\parallel}^{\frac{3}{2}}} \left|\boldsymbol{\nabla}\cdot\boldsymbol{\xi}_\perp + \boldsymbol{\kappa}\cdot\boldsymbol{\xi}_\perp\right|^2 \left(1 - \chi^4\right) |\chi| \left[\frac{\chi^2}{T_{j\parallel}} + \frac{1-\chi^2}{T_{j\perp}}\right]^{-\frac{7}{2}} d\chi d\Psi. \tag{37}$$

Another consequence of the lack of a frequency resonance fraction is that, unlike the kinetic term, the anisotropy term makes no distinction between ions and electrons (as long as $n_i \approx n_e$ and $T_i \approx T_e$). Finally, since $|\chi| \leq 1$, δW_{A2}^{bM} is positive (and therefore stabilizing), when $T_{j\parallel}/T_{j\perp} < 1$ and negative (destabilizing) when $T_{j\parallel}/T_{j\perp} > 1$.

B. Energetic Particles: Anisotropic Slowing-down Distribution

For the anisotropic slowing-down case, $\partial f_j/\partial\chi \neq 0$ as well, but rather:

$$\frac{\partial f_j^b}{\partial \chi} = f_j^b \left(-\frac{2}{\delta\chi^2}\right) \left[\frac{\left(\chi - \chi_0\right) e^{-(\chi-\chi_0)^2/\delta\chi^2} + \left(\chi + 2 + \chi_0\right) e^{-(\chi+2+\chi_0)^2/\delta\chi^2} + \left(\chi - 2 + \chi_0\right) e^{-(\chi-2+\chi_0)^2/\delta\chi^2}}{e^{-(\chi-\chi_0)^2/\delta\chi^2} + e^{-(\chi+2+\chi_0)^2/\delta\chi^2} + e^{-(\chi-2+\chi_0)^2/\delta\chi^2}}\right]. \tag{38}$$

The expression for δW_{A2}^b then results from substituting $\partial f_j^b/\partial\chi$ into Eq. 34.

VII. Calculations Using the MISK Code

The fluid, anisotropy, and kinetic δW terms will be calculated numerically for an NSTX equilibrium in four steps. First, δW_F is what is normally calculated by the PEST code (as long as we assume that $p_{\rm avg} = p$). Second, the $\sigma - 1$ terms of δW_A can be calculated through a modification of PEST which separates out the various stabilizing and destabilizing terms, and multiplies the three relevant terms by $\mu_0(p_\perp - p_\parallel)/B^2$ inside the volume integral of Eq. 17. The integration of this quantity is performed by summation over surfaces and poloidal harmonics on each surface.

Finally, in steps three and four, the MISK code is used to calculate δW_K and δW_{A2} according to the methods outlined in Secs. V and VI. MISK has been used previously for various machines to calculate kinetic effects on stability of Maxwellian thermal particles[8–10,12,43,57–60] as well as for isotropic or simple anisotropic distributions of trapped energetic particles[10,57–60]. Here it is expanded to include the anisotropic bi-Maxwellian distribution for thermal particles, the $\sigma - 1$ fluid corrections, the δW_{A2} correction to the pressure-driven ballooning destabilization term, circulating energetic particles, and an expansion of the anisotropic slowing-down distribution to allow for $\chi_0(\Psi)$ and $\delta\chi(\Psi, \varepsilon)$, in general.

Again it should be noted that the equilibria used in these calculations are themselves purely isotropic. As outlined in Sec. III this approach is valid as long as the anisotropy is considered to be a small perturbation.

A. The Effect of Thermal Particle Pressure Anisotropy - Solov'ev Analytical Equilibrium

For the present study we wish to determine the effect of changing $T_\parallel/T_\perp$ of thermal particles on RWM stability generally. In principle this could be a Ψ dependent quantity, but for simplicity we will use constant ratios across

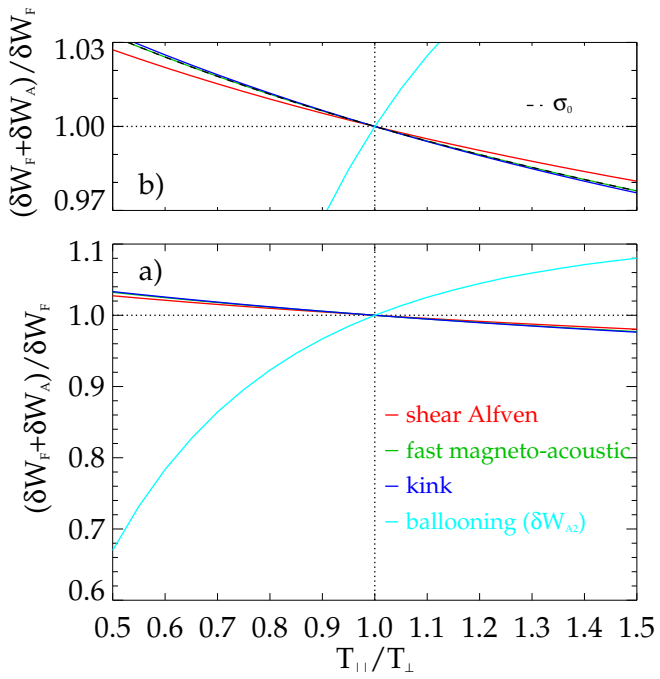

FIG. 2. (Color online) a) $(\delta W_F + \delta W_A^{bM})/\delta W_F$ vs. scaled $T_\parallel/T_\perp$ for the Solov'ev equilibrium. Modification of the pressure-driven ballooning term has a dominant effect. b) is a zoom-in of frame a) showing how the kink, fast magneto-acoustic, and shear Alfvén $\delta W_A/\delta W_F$ terms scale very similarly to $\sigma_0 - 1$.

the entire radial profile. This is an artificial situation, not based on an experimental reality, but it will give insight into the general effect of thermal particle anisotropy. To that end, in this section we will use an analytical Solov'ev equilibrium solution to the Grad-Shafranov equation[61,62] and scan $T_\parallel/T_\perp$ while keeping the total pressure constant. We will use an equilibrium that was also used in Ref. [63]. This equilibrium is shaped, and contains the $q = 2$ and 3 rational surfaces within the plasma, and has a $q_{\rm edge} = 3.263$. It is specified by the parameters $\kappa = 1.6$, $q_0 = 1.9$, and $\epsilon_a = 0.33$ in Eqs. (22) and (23) of Ref. [63].

We will assume that there are no energetic particles, only thermal ions and electrons, and that $n_e = n_i$. Also, for the purposes of determining P for the Solov'ev equilibrium, we now set $R_0 = 1$m and $B_0 = 1$T. Then the total pressure has the form $P = P_0(1 - \psi_n)$, with $P_0 = 4.273 \times 10^4$ Pa. Next we must specify the density profile $n(\Psi)$. We will use $n = n_0(1 - 0.7\Psi_n)$. Then the density on axis, n_0, is determined by specifying $(\omega_{ci}/\omega_A)_0$, where $\omega_{A0} = B_0/(R_0\sqrt{\mu_0 m_i n_{i0}})$ and $\omega_{ci0} = eB_0/m_i = 47.906$ MHz. For the comparisons here, we will use $(\omega_{ci}/\omega_A)_0 = 121$, to be consistent with Ref. [63], even though this results in the values of $\omega_{A0} = 395.914$ kHz and the unrealistically high density $n_0 = 1.518 \times 10^{21}$ m^{-3}. The isotropic temperature profile is then determined from $T = P/(2n)$. For the Solov'ev case this means $T = (P_0/2n_0)(1 - \Psi_n)/(1 - 0.7\Psi_n)$. Finally, we will use the $E \times B$ frequency profile $\omega_E = \omega_{E0}\,(1 - \Psi_n)$, with $\omega_E/\omega_{A0} = 1 \times 10^{-2}$ or $\omega_{E0} = 3.959$ kHz as a nominal value, and $\nu_{\rm eff} = 0$.

Figure 2 shows $(\delta W_F + \delta W_A^{bM})/\delta W_F$ for the various components of the fluid term, vs. $T_\parallel/T_\perp$. Each component is normalized by its own δW_F, not the total. To first order, the correction to the shear Alfvén, fast magneto-acoustic, and kink terms can be approximated by $\delta W_A/\delta W_F = \sigma_0 - 1$, where σ_0 is the value on axis. Since we have considered $T_\parallel/T_\perp$ to be a constant, pulling the factor $1 - \sigma_0$ out of the integral leaves only a factor of B_0^2/B^2 inside. This factor serves to weight the contribution from the low field regions more heavily, but when integrated over the volume it doesn't have a very large effect. The small differences in the shear Alfvén, fast magneto-acoustic, and kink terms in Fig. 2 are due to differences in their weighting, but overall using a simple factor of $\sigma_0 - 1$ can provide a very good estimate of the anisotropy correction of these terms (unless, of course, $T_\parallel/T_\perp$ is strongly dependent on location).

Not surprisingly, the correction to the pressure-driven ballooning destabilization term is considerably larger than $\sigma_0 - 1$. Here, as opposed to the other cases, lower $T_\parallel/T_\perp$ leads to a smaller total fluid effect. Higher $T_\parallel/T_\perp$ leads to an increased effect, but the increase is not as strong as the decrease at low $T_\parallel/T_\perp$. Like the other terms, the δW_{A2} term is half from ions and half from electrons, and additionally we have found it to be dominated by trapped particles over circulating particles.

Note that Fig. 2 shows normalized quantities. In absolute terms (though arbitrary units), the isotropic contributions to δW_F from shear Alfvén, fast magneto-acoustic, kink, and ballooning were 1.34×10^{-1}, 3.95×10^{-4}, -2.24×10^{-1}, and

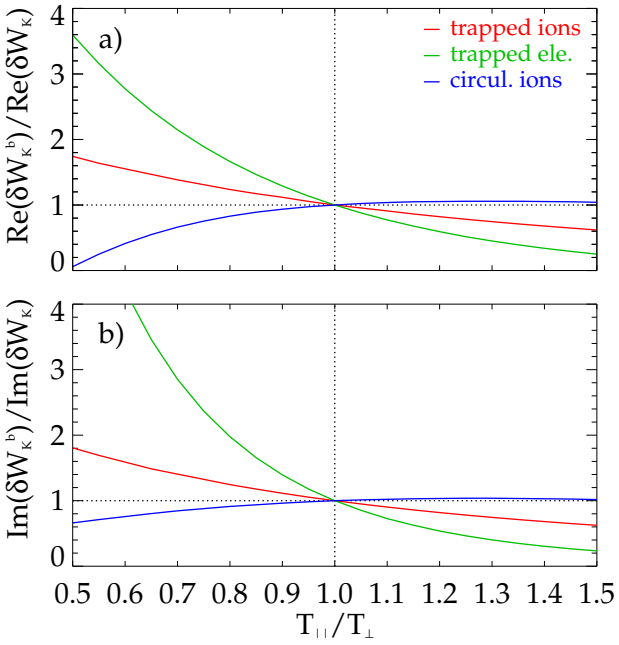

FIG. 3. (Color online) a) Real and b) imaginary components of δW_K normalized by the isotropic δW_K vs. scaled $T_\parallel/T_\perp$ for the Solov'ev equilibrium. The effect of anisotropy of three particles types, trapped ions and electrons and circulating ions, are shown.

-4.35×10^{-2}, respectively. Therefore, while the changes to the shear Alfvén, fast magneto-acoustic, and kink terms are essentially the same in a relative sense, the fast magneto-acoustic term is quite small in this case, and therefore unimportant. Also the shear Alfvén term is stabilizing, and therefore positive, while the kink term is destabilizing, and therefore negative. Therefore the corrections to these two terms partially offset each other. Finally, even though the correction to the ballooning term was considerably larger in a relative sense, in this case it is actually only one third of the shear Alfvén and one fifth of the kink term.

The kinetic effects for thermal particles are calculated with Eq. 18, resulting in both real and imaginary parts. Figure 3 shows these contributions, normalized by their isotropic cases, plotted vs. $T_\parallel/T_\perp$. Three particle types, trapped ions and electrons and circulating ions, are shown separately (the contribution from circulating electrons is usually very small[8]). Generally, increased $Re(\delta W_K)$ is stabilizing, while increased $|Im(\delta W_K)|$ is always stabilizing (see Fig. 1), and for this particular Solov'ev case each of the three components was positive. Therefore in Fig. 3 we can interpret values greater than one as stabilizing and less than one as destabilizing, with respect to the isotropic case. Check the sign of the circulating ion calculation. Trapped ion and electron kinetic stabilizing effects are enhanced when $T_\parallel < T_\perp$ and vice versa. Circulating ion stabilizing kinetic effects are reduced at $T_\parallel/T_\perp < 1$ and little changed above one. The difference between the trapped and circulating ion behavior with respect to $T_\parallel/T_\perp$ comes from the ω_{*T} terms in the numerator of Eq. 24, which taken together tend to be smaller than the isotropic $(\varepsilon/T_j - \frac{3}{2})\omega_{*T}$ for $T_\parallel/T_\perp < 1$ and χ near 1 (circulating particles) and larger than the isotropic value for $T_\parallel/T_\perp < 1$ and χ near 0 (trapped particles). Finally, although the electron term changes more in a relative sense, again these are normalized quantities and in this case (and usually) the trapped thermal ion term is dominant. Additionally, here collisions were not considered. Collisions tend to greatly reduce the electron term[57].

Using Eq. 1, we can finally calculate the predicted growth rate of the RWM and plot it vs. $T_\parallel/T_\perp$ in Fig. 4. First, without considering kinetic effects, we can see the effect of the fluid anisotropy corrections on the fluid growth rate. The effect of only the ballooning term δW_{A2} is shown in red, and of all the terms in green, showing that the ballooning term is the dominant fluid anisotropy correction. Once again, we see that lower $T_\parallel/T_\perp$ is stabilizing and higher $T_\parallel/T_\perp$ is destabilizing, which follows from Fig. 2. When anisotropic kinetic effects are included, but not the fluid effects, the plasma becomes more stable ($\gamma\tau_w \approx 0.43 \rightarrow 0.30$ in the isotropic case), and lower $T_\parallel/T_\perp$ is stabilizing, following from Fig. 3 with trapped thermal ions dominant. When the kinetic and fluid corrections are both applied, the effect is even more enhanced.

Overall the biggest effect on RWM stability from anisotropy of the thermal particles will be in plasmas with high beta (where σ can be large), a large pressure-driven ballooning instability drive, and with $T_\perp$ larger than $T_\parallel$. In this

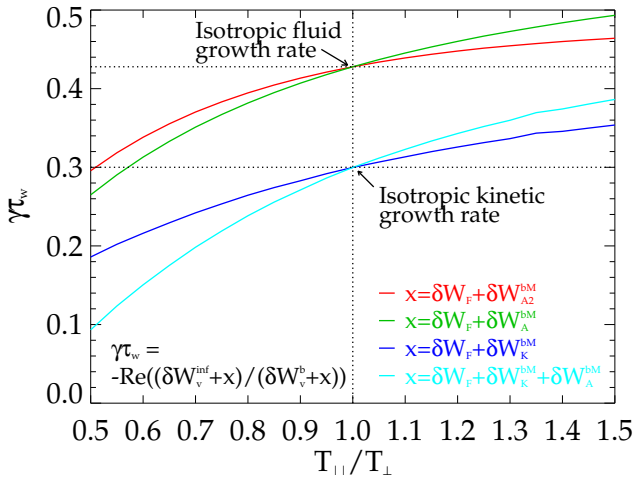

FIG. 4. (Color online) The effect of anisotropy of thermal particles on the RWM growth rate for the Solov'ev equilibrium. The growth rate normalized to the wall time is given by $\gamma\tau_w = -Re((\delta W_v^\infty + x)/(\delta W_v^b + x))$. Shown is the isotropic fluid growth rate ($x = \delta W_F$) and two modifications to it: including only the ballooning term ($x = \delta W_F + \delta W_{A2}^{bM}$) or all the anisotropic fluid corrections ($x = \delta W_F + \delta W_A^{bM}$). Also shown is the isotropic kinetic growth rate ($x = \delta W_F + \delta W_K$) and two modifications to it: including only the anisotropic kinetic term ($x = \delta W_F + \delta W_K^{bM}$) or including both the fluid and kinetic corrections ($x = \delta W_F + \delta W_A^{bM} + \delta W_K^{bM}$).

case a reduction of the ballooning destabilization term can be expected, as well as an enhancement of the stabilizing kinetic effects of the trapped thermal ions.

B. The Effect of Energetic Particle Pressure Anisotropy

To explore the dependence of RWM stability on the anisotropy of energetic particles, we will now use a real experimental equilibrium from NSTX (shot 121090 at 0.601s) which has energetic ions from neutral beam injection. The thermal particles will be considered Maxwellian (contributing a δW_K^M). Figure 5 shows the energetic particle distribution function for the NSTX equilibrium near the core ($r/a = 0.05$), as calculated by `TRANSP`[64] and modeled by Eq. 25 for f_j^b with $\chi_0 = 0.5$ and $\delta\chi_0 = 0.2$. More details of this figure and future improvements to the model are discussed separately in the next section (Sec. VIII). For the purposes of the remainder of this section, we will now proceed by considering $\chi_0(\Psi)$ and $\delta\chi_0(\Psi)$ to be constants, even if this may not provide the best match to experimental conditions, in order to parameterize the effect of energetic particle anisotropy on these two parameters. $\chi_0 = 0$ is akin to perpendicular beam injection, and $\chi_0 = 1$ to parallel; smaller $\delta\chi_0$ indicates a more narrow distribution while larger $\delta\chi_0$ is getting closer to the isotropic case. The study performed here, looking at the effect of the injection pitch angle and the breadth of the pitch angle spread, is complimentary to a previous one (Ref. [15]) which looked at the effect of the beam injection energy and a changing deposition location in Ψ (such as might come from an off-axis neutral beam).

Note that the distribution function does contain a Ψ dependence through $\hat{\varepsilon}$ (through $T_e(\Psi)$), and of course through the density $n_j(\Psi)$. We will not alter these quantities, however, using the experimental T_e profile, and `TRANSP` calculated energetic particle density profile. Whereas previously (Ref. [10]) $p_j(\Psi)$ was also taken from `TRANSP` for the beam ion pressure, and then an $\varepsilon_b(\Psi)$ profile consistent with the `TRANSP` density and pressure and our distribution function model was determined, here we use only $n_j(\Psi)$ from `TRANSP` and constant, known ε_b for the beams. This effectively determines $p_j(\Psi)$, which may differ from what `TRANSP` determines for $p_j(\Psi)$.

Let us now proceed to discuss the impact of energetic particle anisotropy on the fluid terms. Here we will consider $\sigma - 1 \approx 0$ in order to concentrate on the ballooning term, which is the most important. Figures 6-8 show contours of $\gamma\tau_w = -Re((\delta W_V^\infty + x)/(\delta W_V^b))$ vs. scaled constant χ_0 and $\delta\chi_0$. For thermal particles only $x = x_{th} = \delta W_F + \delta W_K^M$. In these figures the range of χ_0 from 0 to 1 is shown, but the effects are exactly the same for counter-injection (-1 to 0), which can be seen from careful examination of Eqs. 30, 31, and 38.

Figure 6 shows $\gamma\tau_w$ with $x = x_{th} + \delta W_{A2}$, ie. it includes only the ballooning correction. Figure 6 includes both trapped and circulating energetic particles, but as in the bi-Maxwellian case, we find that δW_{A2} is dominated by trapped particles. Due to the $(\chi^4 - 1)(\partial f_j/\partial\chi)$ term in Eq. 34, trapped energetic particles at small χ are emphasized.

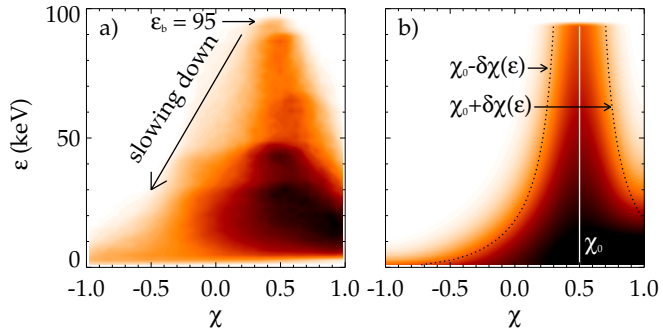

FIG. 5. (Color online) Contours of the distribution function f_j^b of energetic particles in NSTX shot 121090 at 0.6s, at the surface with $r/a = 0.05$ a) as determined by TRANSP, and b) as modeled by Eq. 25 with $\chi_0 = 0.5$ and $\delta\chi_0 = 0.2$.

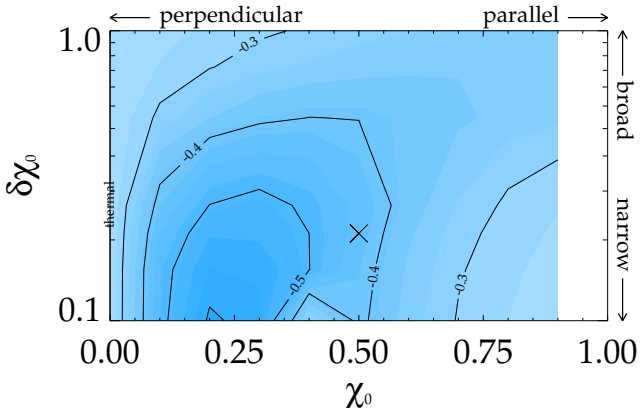

FIG. 6. (Color online) Contours of $\gamma\tau_w$ including δW_{A2} and δW_K^M (thermal particles), but not δW_K^b (energetic particles) for trapped and circulating energetic particles in the NSTX equilibrium, where the anisotropic slowing-down distribution function is described by scaled constant χ_0 and $\delta\chi_0$. $\chi_0 = 0$ is akin to perpendicular beam injection, and $\chi_0 = 1$ to parallel. Smaller $\delta\chi_0$ indicates a more narrow distribution while larger $\delta\chi_0$ is getting closer to the isotropic case. The approximate NSTX experimental values from Fig. 5 are marked with a $\times$ symbol.

There tends to be a sharp gradient of the distribution at small χ when the injection pitch is near there (perpendicular injection, χ_0 near 0), and a flatter $\partial f_j/\partial\chi$ at small χ when the injection is more perpendicular. This accounts for the larger δW_{A2} at smaller χ_0. However, $\partial f_j/\partial\chi$ is symmetric in χ when $\chi_0 = 0$, so when the injection is perfectly perpendicular $\delta W_{A2} = 0$. The net result is that the contribution from δW_{A2} peaks near $\chi_0 = 0.25$. Finally, in general more narrow distributions (smaller $\delta\chi_0$) means a larger $\partial f_j/\partial\chi$ and therefore a larger δW_{A2}, while as $\delta\chi_0 \to \infty$ in the isotropic case, the derivative and δW_{A2} are zero. Overall, we can see that the stabilizing anisotropic correction to the ballooning term can be quite significant; at the approximate NSTX values of $\chi_0 = 0.5$, $\delta\chi_0 = 0.2$ (see Fig. 5), $\gamma\tau_w$ is quite stable ($-0.4X$ vs. the value with thermal particles only of -0.24), and a more perpendicular injection could provide an even larger stability increment.

Figure 7 once again shows contours of $\gamma\tau_w$ vs. scaled constant χ_0 and $\delta\chi_0$. This time $x = x_{th} + \delta W_K^b$, ie. the anisotropic energetic particle's kinetic effects are included but δW_{A2} is not. Also here we are showing separately the real and imaginary contributions to δW_K^b, for trapped and circulating energetic particles. For trapped particles the real part is destabilizing at low χ_0 and stabilizing at larger χ_0, while the imaginary part is strongly stabilizing at low χ_0. For circulating particles, the real part is more stabilizing at larger χ_0, while the imaginary part is stabilizing at high χ_0 and destabilizing at lower χ_0. In every case the effects are amplified by a more narrow distribution (lower $\delta\chi_0$). Such a complex picture of the effect of beam ion injection angle on RWM stability could not have been determined by examination of Eqs. 19, 30, and 31, but comes though with the full calculation. For the approximate NSTX case marked in the figure, the energetic particles are about $3-5\%$ stabilizing in three cases and destabilizing in one.

Finally, putting all the terms together, Fig. 8 shows the growth rate vs. scaled constant χ_0 and $\delta\chi_0$, with the ballooning anisotropy fluid correction and anisotropic kinetic effects both taken into account (essentially the additive effect of Figs. 6 and 7a-d). Altogether, the stabilizing effect of the energetic particles is between $15-40\%$ (17% for the NSTX case) compared to the thermal particle only case. The stabilizing effect is greatest for narrow beam spreading

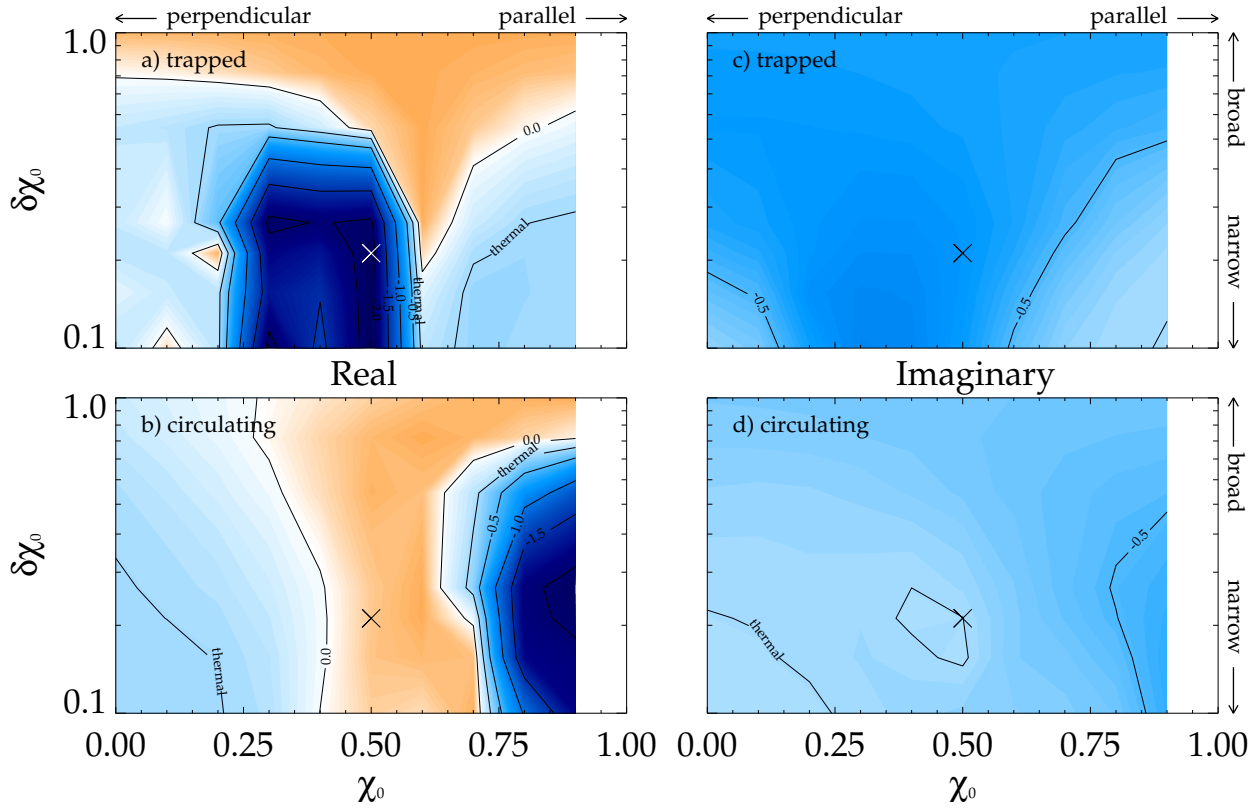

FIG. 7. (Color online) Contours of $\gamma\tau_w$ vs. scaled constant χ_0 and $\delta\chi_0$, where $\gamma\tau_w$ includes δW_K^M and a) $Re(\delta W_K^b)$ for trapped energetic particles, b) $Re(\delta W_K^b)$ for circulating energetic particles, c) $Im(\delta W_K^b)$ for trapped energetic particles, and d) $Im(\delta W_K^b)$ for circulating energetic particles in the NSTX equilibrium. The approximate NSTX experimental values from Fig. 5 are marked with a $\times$ symbol. A contour of $(\gamma\tau_w)_{th} = -0.24$ for the thermal particle only case is marked for comparison.

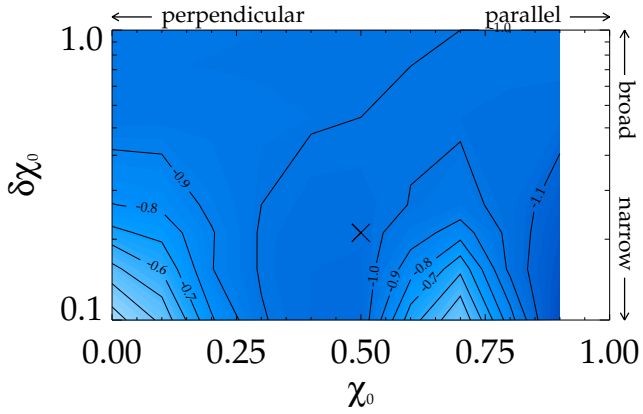

FIG. 8. (Color online) Contours of $\gamma\tau_w$ vs. scaled constant χ_0 and $\delta\chi_0$, where $\gamma\tau_w$ includes δW_K^M, δW_{A2}, and δW_K^b. The approximate NSTX experimental values from Fig. 5 are marked with a $\times$ symbol.

and an injection pitch of about 0.25, due mostly to the δW_{A2} ballooning correction and the $Im(\delta W_K^b)$ for trapped energetic particles.

VIII. FURTHER IMPROVEMENTS TO THE ENERGETIC PARTICLE DISTRIBUTION FUNCTION MODEL

In this work both χ_0 and $\delta\chi_0$ in the anisotropic slowing-down distribution function were considered constants for the sake of simplified discussion and plotting of Figs. 6-8. It is straightforward to allow each of these quantities to be a factor of Ψ, the surface coordinate. Secondly, Eq. 25 for f_j^b can be made more general by making it a sum of many different particle types, so that if, for example, there are s number of beam sources, k number of energy components, and p surfaces of deposition, the total energetic particle distribution is fully described by the linear superposition of $s \times k \times p$ separate distributions of the form of Eq. 25. In NSTX this means up to 3 beam sources, with 3 energy components (full, half and one-third), and 2 surfaces of deposition each, for a possible total of 18 different f_j^b terms. As an example, in Fig. 5a, the beam energy was 95 keV, and one can see that steps in f_j^b at 42.5 keV and 31.7 keV are not reflected in the model in Fig. 5b. Also, the present model does a better job near the axis, because towards the edge the splitting of the beam deposition into two pitch angles (two χ_0s, where the beam enters and exits the surface) becomes more pronounced. Fortunately energetic particle density is higher near the axis, making these particles more important to accurately model. Use of multiple, superposed distribution functions may become necessary, however, to accurately model the energetic particles in NSTX-U, which will have a second, off-axis neutral beam, or for DIII-D, which has multiple beams including one that can be tilted. Additionally, ITER will have multiple important heating sources[65,66], which may affect the energetic particle distribution in an even more complex way.

IX. CONCLUSIONS AND PHYSICAL IMPLICATIONS

We have derived the effect of anisotropy of the plasma pressure on the resistive wall mode stability energy principle. The fluid anisotropy has been treated as a small perturbation on the plasma equilibrium, which allows a relatively simple treatment of the problem. Fluid treatment with CGL pressures is akin to consideration of the high frequency mode rotation limit. More complete treatment leads to kinetic terms in addition to anisotropy corrections to the fluid terms. Specifically, the shear Alfvén, fast magneto-acoustic, and kink fluid terms are relatively simply modified by a factor of σ. Because of the equilibrium considerations in the perturbative approach, these corrections are necessarily small in our treatment. The kinetic effects depend upon $\partial f/\partial\varepsilon$ and $\partial f/\partial\Psi$, while the anisotropy correction to the fluid pressure-driven ballooning term depends upon $\partial f/\partial\chi$. We have derived expressions for these terms for a perturbed bi-Maxwellian distribution function for thermal particles and an anisotropic slowing-down distribution for energetic particles

For thermal particles with $T_\perp$ larger than $T_\parallel$ the ballooning destabilization term is reduced while the stabilizing kinetic effects of the trapped thermal ions are enhanced, leading to an increase in RWM stability. Note, however, that in the analysis presented here (for an analytical Solov'ev equilibrium) $T_\parallel/T_\perp$ was assumed to be changed over the whole plasma volume, and had to be relatively significantly different from unity to see a large effect. Such a scenario would be difficult to achieve in experimental reality. In this light, the effect of realistic thermal particle anisotropy on RWM stability is likely to be quite modest. Extension of this relevant physics to less global modes, such as sawteeth, is possible, however.

For energetic particles we have concentrated on calculation of the effect of anisotropic slowing-down beam ions on NSTX stability, as well as the consequences of perpendicular vs. parallel injection and broad vs. narrow spreading in pitch angle. The ballooning term is modified to be less destabilizing, especially for beam ions with injection pitch angle of about 0.25 and a narrow spread. The kinetic effect from the anisotropic energetic particles is complex, and made up of real and imaginary trapped and circulating parts. Generally, the overall effect of beam ions is to be significantly stabilizing, but the degree of which depends on the injection pitch and width of spread, again maximizing at $\chi_0 \approx 0.25$ and small $\delta\chi_0$. One major caveat to this analysis is that the beams impart momentum, so changing their injection to a more perpendicular angle will inevitably reduce the total plasma rotation. This type of self-consistent analysis has not been attempted here (rotation was held constant at the experimental value), but would be important for a full understanding of the impact of beam ions on RWM stability.

ACKNOWLEDGMENTS

This research was supported by the U.S. Department of Energy under contracts DE-FG02-99ER54524, DE-AC02-09CH11466, and DE-FG02-93ER54215.

Appendix A: Derivation of CGL Perturbed Fluid Pressures Using Double-Polytropic Laws

This section is should not be included

The perturbed fluid pressures, $\tilde{p}_\perp$ and $\tilde{p}_\parallel$ can be derived by using double-polytropic laws[67,68] as replacements for the adiabatic equation: $d(p_\parallel B^{\gamma_\parallel - 1}\rho^{-\gamma_\parallel})/dt = 0$, and $d(p_\perp B^{1-\gamma_\perp}\rho^{-1})/dt = 0$. The CGL double-adiabatic equations[27,30,31,69,70], which are derived from the first and second adiabatic invariants[71] under the assumption of negligible heat flux[72,73] have $\gamma_\parallel = 3$ and $\gamma_\perp = 2$.

From the $p_\parallel$ equation, we find[68,73]:

$$\frac{\partial p_\parallel}{\partial t} + \mathbf{v}\cdot\boldsymbol{\nabla} p_\parallel = -\left(\gamma_\parallel - 1\right)\frac{p_\parallel}{B}\hat{\mathbf{b}}\cdot\left(\frac{\partial \mathbf{B}}{\partial t} + \mathbf{v}\cdot\boldsymbol{\nabla}\mathbf{B}\right) + \gamma_\parallel\frac{p_\parallel}{\rho}\left(\frac{\partial \rho}{\partial t} + \mathbf{v}\cdot\boldsymbol{\nabla}\rho\right) \tag{A1}$$

$$\left(-i\omega + \mathbf{v_0}\cdot\boldsymbol{\nabla}\right)\tilde{p}_\parallel + \tilde{\mathbf{v}}\cdot\boldsymbol{\nabla} p_\parallel = -\left(\gamma_\parallel - 1\right)\frac{p_\parallel}{B}\hat{\mathbf{b}}\cdot\left(\left(-i\omega + \mathbf{v_0}\cdot\boldsymbol{\nabla}\right)\tilde{\mathbf{B}} + \tilde{\mathbf{v}}\cdot\boldsymbol{\nabla}\mathbf{B_0}\right) + \gamma_\parallel\frac{p_\parallel}{\rho}\left(\left(-i\omega + \mathbf{v_0}\cdot\boldsymbol{\nabla}\right)\tilde{\rho} + \tilde{\mathbf{v}}\cdot\boldsymbol{\nabla}\rho_0\right) \tag{A2}$$

$$\left(-i\omega + \mathbf{v_0}\cdot\boldsymbol{\nabla}\right)\left(\tilde{p}_\parallel + \boldsymbol{\xi}_\perp\cdot\boldsymbol{\nabla} p_\parallel\right) = \left(-i\omega + \mathbf{v_0}\cdot\boldsymbol{\nabla}\right)\left[-\left(\gamma_\parallel - 1\right)\frac{p_\parallel}{B}\hat{\mathbf{b}}\cdot\left(\tilde{\mathbf{B}} + \boldsymbol{\xi}_\perp\cdot\boldsymbol{\nabla}\mathbf{B_0}\right) + \gamma_\parallel\frac{p_\parallel}{\rho}\left(\tilde{\rho} + \boldsymbol{\xi}_\perp\cdot\boldsymbol{\nabla}\rho_0\right)\right] \tag{A3}$$

Now using $\tilde{\mathbf{B}} = \boldsymbol{\nabla}\times\left(\boldsymbol{\xi}_\perp\times\mathbf{B_0}\right) = -\mathbf{B_0}(\boldsymbol{\nabla}\cdot\boldsymbol{\xi}_\perp)$ and $\tilde{\rho} = -\rho_0\boldsymbol{\nabla}\cdot\boldsymbol{\xi}_\perp - \left(\boldsymbol{\xi}_\perp\cdot\boldsymbol{\nabla}\right)\rho_0$, we have:

$$\tilde{p}_\parallel = -\boldsymbol{\xi}_\perp\cdot\boldsymbol{\nabla} p_\parallel - \left(\gamma_\parallel - 1\right)\frac{p_\parallel}{B}\hat{\mathbf{b}}\cdot\left(-\mathbf{B_0}\left(\boldsymbol{\nabla}\cdot\boldsymbol{\xi}_\perp\right) + \boldsymbol{\xi}_\perp\cdot\boldsymbol{\nabla}\mathbf{B_0}\right) + \gamma_\parallel\frac{p_\parallel}{\rho}\left(-\rho_0\boldsymbol{\nabla}\cdot\boldsymbol{\xi}_\perp\right) \tag{A4}$$

$$= -\boldsymbol{\xi}_\perp\cdot\boldsymbol{\nabla} p_\parallel - \left(\gamma_\parallel - 1\right)p_\parallel\left(\boldsymbol{\kappa}\cdot\boldsymbol{\xi}_\perp - \boldsymbol{\nabla}\cdot\boldsymbol{\xi}_\perp\right) - \gamma_\parallel p_\parallel\boldsymbol{\nabla}\cdot\boldsymbol{\xi}_\perp \tag{A5}$$

$$= -\boldsymbol{\xi}_\perp\cdot\boldsymbol{\nabla} p_\parallel - p_\parallel\boldsymbol{\nabla}\cdot\boldsymbol{\xi}_\perp + \left(1 - \gamma_\parallel\right)p_\parallel\boldsymbol{\kappa}\cdot\boldsymbol{\xi}_\perp. \tag{A6}$$

Similarly, for $p_\perp$,

$$\tilde{p}_\perp = -\boldsymbol{\xi}_\perp\cdot\boldsymbol{\nabla} p_\perp - \left(1 - \gamma_\perp\right)p_\perp\left(\boldsymbol{\kappa}\cdot\boldsymbol{\xi}_\perp - \boldsymbol{\nabla}\cdot\boldsymbol{\xi}_\perp\right) - p_\perp\boldsymbol{\nabla}\cdot\boldsymbol{\xi}_\perp \tag{A7}$$

$$= -\boldsymbol{\xi}_\perp\cdot\boldsymbol{\nabla} p_\perp - \gamma_\perp p_\perp\boldsymbol{\nabla}\cdot\boldsymbol{\xi}_\perp + \left(\gamma_\perp - 1\right)p_\perp\boldsymbol{\kappa}\cdot\boldsymbol{\xi}_\perp. \tag{A8}$$

For the CGL case this leads finally to:

$$\tilde{p}_\parallel = -\boldsymbol{\xi}_\perp\cdot\boldsymbol{\nabla} p_\parallel - p_\parallel\boldsymbol{\nabla}\cdot\boldsymbol{\xi}_\perp - 2p_\parallel\boldsymbol{\kappa}\cdot\boldsymbol{\xi}_\perp, \tag{A9}$$

$$\tilde{p}_\perp = -\boldsymbol{\xi}_\perp\cdot\boldsymbol{\nabla} p_\perp - 2p_\perp\boldsymbol{\nabla}\cdot\boldsymbol{\xi}_\perp + p_\perp\boldsymbol{\kappa}\cdot\boldsymbol{\xi}_\perp. \tag{A10}$$

Appendix B: Derivation of CGL Perturbed Fluid Pressures Using the High Frequency Limit of the Perturbed Distribution Function.

The perturbed fluid pressures, $\tilde{p}_\perp$ and $\tilde{p}_\parallel$ can be derived by using double-polytropic laws[67,68] as replacements for the adiabatic equation: $d(p_\parallel B^{\gamma_\parallel - 1}\rho^{-\gamma_\parallel})/dt = 0$, and $d(p_\perp B^{1-\gamma_\perp}\rho^{-1})/dt = 0$. The CGL double-adiabatic equations[27,30,31,69,70], which are derived from the first and second adiabatic invariants[71] under the assumption of negligible heat flux[72,73] have $\gamma_\parallel = 3$ and $\gamma_\perp = 2$. Here we will demonstrate that in fact the CGL $\tilde{p}_\perp$ and $\tilde{p}_\parallel$ expressions can also be recovered from Eq. 12 (neglecting the electrostatic contribution) using a bi-Maxwellian equilibrium distribution function and our form of $\tilde{f}_j$ from Eq. 13, with the assumption of fast mode rotation.

Let us now examine $\tilde{f}_j$ in the limit of large ω (which in reality pertains to high frequency modes, *not the RWM*). Then we can take a gyro-average ($\langle\cdot\rangle$) of f_j and in Eq. 13, $\omega(\partial f_j/\partial\varepsilon) \gg n(\partial f_j/\partial P_\phi)$, $\langle\mathbf{v}_\perp\cdot\boldsymbol{\xi}_\perp\rangle = 0$, $\langle\mathbf{v}_\perp\cdot\tilde{\mathbf{B}}\rangle = 0$ and

$$\langle\tilde{s}_j\rangle = \langle\int_{-\infty}^{t}\left(\mathbf{v}\cdot\frac{d\boldsymbol{\xi}_\perp}{dt'} - \frac{\tilde{\boldsymbol{\mathcal{Z}}}}{m_j}\right)dt'\rangle \approx \frac{\langle HT_j\rangle}{im_j\omega}, \tag{B1}$$

so that:

$$\tilde{f}_j^{\omega\to\infty} = -\boldsymbol{\xi}_\perp\cdot\boldsymbol{\nabla} f_j - \frac{\partial f_j}{\partial\varepsilon}\left(\langle HT_j\rangle - Z_j e\left(\tilde{\boldsymbol{\Phi}} + \boldsymbol{\xi}_\perp\cdot\boldsymbol{\nabla}\Phi_0\right)\right) - \mu\frac{\tilde{\mathbf{B}}_\parallel}{B}\frac{\partial f_j}{\partial\mu}. \tag{B2}$$

Now,

$$\tilde{f}_j^{\omega\to\infty} + \frac{\partial f_j}{\partial B}\boldsymbol{\xi}_\perp\cdot\boldsymbol{\nabla}\mathbf{B} = -\boldsymbol{\xi}_\perp\cdot\boldsymbol{\nabla} f_j - \frac{\partial f_j}{\partial\varepsilon}\left(\langle HT_j\rangle - \tilde{\boldsymbol{\mathcal{Z}}}\right) - \frac{\mu}{B}\frac{\partial f_j}{\partial\mu}\left(\tilde{\mathbf{B}}_\parallel + \boldsymbol{\xi}_\perp\cdot\boldsymbol{\nabla}\mathbf{B}\right) \tag{B3}$$

$$= -\boldsymbol{\xi}_\perp\cdot\boldsymbol{\nabla} f_j - m_j\frac{\partial f_j}{\partial\varepsilon}\left(\frac{1}{2}v_\perp^2\boldsymbol{\nabla}\cdot\boldsymbol{\xi}_\perp + \frac{1}{2}v_\perp^2\boldsymbol{\kappa}\cdot\boldsymbol{\xi}_\perp - v_\parallel^2\boldsymbol{\kappa}\cdot\boldsymbol{\xi}_\perp\right) - \mu\frac{\partial f_j}{\partial\mu}\left(\boldsymbol{\kappa}\cdot\boldsymbol{\xi}_\perp + \boldsymbol{\nabla}\cdot\boldsymbol{\xi}_\perp\right), \tag{B4}$$

where in the last line we have used Eq. 6 of Ref. [12] for $\langle H\rangle$ and $\tilde{\mathbf{B}}_\parallel = -B\left(\boldsymbol{\nabla}\cdot\boldsymbol{\xi}_\perp + \boldsymbol{\kappa}\cdot\boldsymbol{\xi}_\perp\right) - \hat{\mathbf{b}}\cdot\boldsymbol{\xi}_\perp\cdot\boldsymbol{\nabla}\mathbf{B}$.

From Eq. 21 for the bi-Maxwellian distribution $\partial f_j/\partial\varepsilon = -f_j/T_{j\parallel}$, and $\partial f_j/\partial\mu = -f_j B\left(\frac{1}{T_{j\perp}} - \frac{1}{T_{j\parallel}}\right)$. Now making these substitutions we find that:

$$\tilde{f}_j^{\omega\to\infty} + \frac{\partial f_j}{\partial B}\boldsymbol{\xi}_\perp\cdot\boldsymbol{\nabla}\mathbf{B} = -\boldsymbol{\xi}_\perp\cdot\boldsymbol{\nabla} f_j + f_j m_j\left[\frac{1}{T_{j\parallel}}\left(-v_\parallel^2\boldsymbol{\kappa}\cdot\boldsymbol{\xi}_\perp\right) + \frac{1}{T_{j\perp}}\left(\frac{1}{2}v_\perp^2\boldsymbol{\kappa}\cdot\boldsymbol{\xi}_\perp - \frac{1}{2}v_\perp^2\boldsymbol{\nabla}\cdot\boldsymbol{\xi}_\perp\right)\right]. \tag{B5}$$

We then define the quantities R_1, R_2, and R_3 as in Ref. [74]:

$$R_1 = \sum_j m_j\int v_\parallel^4 f_j d^3\mathbf{v} = \frac{3p_\parallel^2}{\rho}, \tag{B6}$$

$$R_2 = \frac{1}{2}\sum_j m_j\int v_\parallel^2 v_\perp^2 f_j d^3\mathbf{v} = \frac{p_\parallel p_\perp}{\rho}, \tag{B7}$$

$$R_3 = \frac{1}{2}\sum_j m_j\int v_\perp^4 f_j d^3\mathbf{v} = \frac{4p_\perp^2}{\rho}. \tag{B8}$$

Now from Eq. 12

$$\tilde{p}_\parallel = \sum_j m_j\int v_\parallel^2\left(\tilde{f}_j^{\omega\to\infty} + \frac{\partial f_j}{\partial B}\boldsymbol{\xi}_\perp\cdot\boldsymbol{\nabla}\mathbf{B}\right)d^3\mathbf{v} \tag{B9}$$

$$= -\boldsymbol{\xi}_\perp\cdot\boldsymbol{\nabla} p_\parallel - \frac{m_j}{T_{j\parallel}}R_1\boldsymbol{\kappa}\cdot\boldsymbol{\xi}_\perp + \frac{m_j}{T_{j\perp}}R_2\boldsymbol{\kappa}\cdot\boldsymbol{\xi}_\perp - \frac{m_j}{T_{j\perp}}R_2\boldsymbol{\nabla}\cdot\boldsymbol{\xi}_\perp \tag{B10}$$

$$= -\boldsymbol{\xi}_\perp\cdot\boldsymbol{\nabla} p_\parallel - p_\parallel\boldsymbol{\nabla}\cdot\boldsymbol{\xi}_\perp - 2p_\parallel\boldsymbol{\kappa}\cdot\boldsymbol{\xi}_\perp, \tag{B11}$$

and

$$\tilde{p}_\perp = \sum_j\frac{1}{2}m_j\int v_\perp^2\left(\tilde{f}_j^{\omega\to\infty} + \frac{\partial f_j}{\partial B}\boldsymbol{\xi}_\perp\cdot\boldsymbol{\nabla}\mathbf{B}\right)d^3\mathbf{v} \tag{B12}$$

$$-\boldsymbol{\xi}_\perp\cdot\boldsymbol{\nabla} p_\perp - \frac{m_j}{T_{j\parallel}}R_2\boldsymbol{\kappa}\cdot\boldsymbol{\xi}_\perp + \frac{m_j}{2T_{j\perp}}R_3\boldsymbol{\kappa}\cdot\boldsymbol{\xi}_\perp - \frac{m_j}{2T_{j\perp}}R_3\boldsymbol{\nabla}\cdot\boldsymbol{\xi}_\perp \tag{B13}$$

$$= -\boldsymbol{\xi}_\perp\cdot\boldsymbol{\nabla} p_\perp - 2p_\perp\boldsymbol{\nabla}\cdot\boldsymbol{\xi}_\perp + p_\perp\boldsymbol{\kappa}\cdot\boldsymbol{\xi}_\perp, \tag{B14}$$

Appendix C: Self-adjointness of the Anisotropic Fluid δW

In order to show that $\delta W_F + \delta W_A$ is self-adjoint, we must look at both the ballooning term from Eq. 16, and the kink term from Eqs. 16 and 17 together. Beginning with the kink term we write:

$$\delta W_{F+A}^{\text{kink}} = \frac{1}{2}\int \frac{\sigma j_\parallel}{2B}\left((\boldsymbol{\xi}_\perp^* \times \mathbf{B})\cdot\tilde{\mathbf{B}}_\perp + (\boldsymbol{\xi}_\perp^* \times \mathbf{B})\cdot\tilde{\mathbf{B}}_\perp\right) d\mathbf{V} \tag{C1}$$

$$= \frac{1}{2}\int \frac{\sigma j_\parallel}{2B}\left((\boldsymbol{\xi}_\perp^* \times \mathbf{B})\cdot\boldsymbol{\nabla}\times(\boldsymbol{\xi}_\perp \times \mathbf{B}) + (\boldsymbol{\xi}_\perp^* \times \mathbf{B})\cdot\tilde{\mathbf{B}}_\perp\right) d\mathbf{V} \tag{C2}$$

$$= \frac{1}{2}\int \frac{\sigma j_\parallel}{2B}\left(\boldsymbol{\nabla}\cdot\left((\boldsymbol{\xi}_\perp \times \boldsymbol{\xi}_\perp^*\cdot\mathbf{B})\,\mathbf{B}\right) + (\boldsymbol{\xi}_\perp \times \mathbf{B})\cdot\boldsymbol{\nabla}\times(\boldsymbol{\xi}_\perp^* \times \mathbf{B}) + (\boldsymbol{\xi}_\perp^* \times \mathbf{B})\cdot\tilde{\mathbf{B}}_\perp\right) d\mathbf{V} \tag{C3}$$

$$= \frac{1}{2}\int \left(\boldsymbol{\nabla}\cdot\left(\frac{\sigma j_\parallel}{2B}(\boldsymbol{\xi}_\perp \times \boldsymbol{\xi}_\perp^*\cdot\mathbf{B})\,\mathbf{B}\right) - (\boldsymbol{\xi}_\perp \times \boldsymbol{\xi}_\perp^*\cdot\mathbf{B})\,\mathbf{B}\cdot\boldsymbol{\nabla}\left(\frac{\sigma j_\parallel}{2B}\right) + \frac{\sigma j_\parallel}{2B}\left((\boldsymbol{\xi}_\perp \times \mathbf{B})\cdot\tilde{\mathbf{B}}_\perp^* + (\boldsymbol{\xi}_\perp^* \times \mathbf{B})\cdot\tilde{\mathbf{B}}_\perp\right)\right) d\mathbf{V}. \tag{C4}$$

The first term integrates to zero over the volume. The last terms together are self-adjoint. Defining $\boldsymbol{\xi}_\perp = \xi_\Psi \hat{\boldsymbol{e}}_{\boldsymbol{\Psi}} + \xi_\chi \hat{\boldsymbol{e}}_{\boldsymbol{\chi}}$, with $\hat{\boldsymbol{e}}_{\boldsymbol{\Psi}} = \boldsymbol{\nabla}\Psi/|\boldsymbol{\nabla}\Psi|$ and $\hat{\boldsymbol{e}}_{\boldsymbol{\chi}} = \hat{\mathbf{b}}\times\boldsymbol{\nabla}\Psi/|\boldsymbol{\nabla}\Psi|$, and rewriting, we have:

$$\delta W_{F+A}^{\text{kink}} = \frac{1}{2}\int \left(\frac{\sigma j_\parallel}{2B}\left((\boldsymbol{\xi}_\perp \times \mathbf{B})\cdot\tilde{\mathbf{B}}_\perp^* + (\boldsymbol{\xi}_\perp^* \times \mathbf{B})\cdot\tilde{\mathbf{B}}_\perp\right) - \left(\boldsymbol{\xi}_{\boldsymbol{\Psi}}\boldsymbol{\xi}_{\boldsymbol{\chi}}^* - \boldsymbol{\xi}_{\boldsymbol{\chi}}\boldsymbol{\xi}_{\boldsymbol{\Psi}}^*\right)\mathbf{B}\boldsymbol{\nabla}\cdot\left(\frac{\sigma j_\parallel}{2}\hat{\mathbf{b}}\right)\right) d\mathbf{V}. \tag{C5}$$

Now let us return to the ballooning term and write:

$$\delta W_{F+A}^{\text{ballooning}} = \int \left(\boldsymbol{\kappa}_{\boldsymbol{\Psi}}\boldsymbol{\xi}_{\boldsymbol{\Psi}}^* + \boldsymbol{\kappa}_{\boldsymbol{\chi}}\boldsymbol{\xi}_{\boldsymbol{\chi}}^*\right)\left(\boldsymbol{\xi}_\perp\cdot\boldsymbol{\nabla}\Psi\frac{\partial p_{\text{avg}}}{\partial\Psi} + \boldsymbol{\xi}_\perp\cdot\boldsymbol{\nabla}B\frac{\partial p_{\text{avg}}}{\partial B}\right) d\mathbf{V} \tag{C6}$$

$$= \int \left(\left(\boldsymbol{\xi}_{\boldsymbol{\Psi}}\boldsymbol{\xi}_{\boldsymbol{\Psi}}^*\boldsymbol{\kappa}_{\boldsymbol{\Psi}} + \boldsymbol{\xi}_{\boldsymbol{\Psi}}\boldsymbol{\xi}_{\boldsymbol{\chi}}^*\boldsymbol{\kappa}_{\boldsymbol{\chi}}\right)\left(|\boldsymbol{\nabla}\Psi|\frac{\partial p_{\text{avg}}}{\partial\Psi} + \hat{\boldsymbol{e}}_{\boldsymbol{\Psi}}\cdot\boldsymbol{\nabla}B\frac{\partial p_{\text{avg}}}{\partial B}\right) + \left(\boldsymbol{\xi}_{\boldsymbol{\chi}}\boldsymbol{\xi}_{\boldsymbol{\chi}}^*\boldsymbol{\kappa}_{\boldsymbol{\chi}} + \boldsymbol{\xi}_{\boldsymbol{\chi}}\boldsymbol{\xi}_{\boldsymbol{\Psi}}^*\boldsymbol{\kappa}_{\boldsymbol{\Psi}}\right)\left(\hat{\boldsymbol{e}}_{\boldsymbol{\chi}}\cdot\boldsymbol{\nabla}B\frac{\partial p_{\text{avg}}}{\partial B}\right)\right) d\mathbf{V}. \tag{C7}$$

Then let us momentarily consider

$$\boldsymbol{\nabla}\times\hat{\mathbf{b}}\cdot\boldsymbol{\nabla}p_{\text{avg}} = \boldsymbol{\nabla}\times\hat{\mathbf{b}}\cdot\boldsymbol{\nabla}\Psi\frac{\partial p_{\text{avg}}}{\partial\Psi} + \boldsymbol{\nabla}\times\hat{\mathbf{b}}\cdot\boldsymbol{\nabla}B\Psi\frac{\partial p_{\text{avg}}}{\partial B} \tag{C8}$$

$$= \boldsymbol{\nabla}\times\hat{\mathbf{b}}\cdot\boldsymbol{\nabla}\Psi\frac{\partial p_{\text{avg}}}{\partial\Psi} + \boldsymbol{\nabla}\times\hat{\mathbf{b}}\cdot\boldsymbol{\nabla}\Psi\frac{\partial B}{\partial\Psi}\frac{\partial p_{\text{avg}}}{\partial B} + \left(\boldsymbol{\nabla}\times\hat{\mathbf{b}}\cdot\hat{\mathbf{b}}\right)\left(\hat{\mathbf{b}}\cdot\boldsymbol{\nabla}B\right)\frac{\partial p_{\text{avg}}}{\partial B} + \left(\boldsymbol{\nabla}\times\hat{\mathbf{b}}\cdot\hat{\boldsymbol{e}}_{\boldsymbol{\chi}}\right)\left(\hat{\boldsymbol{e}}_{\boldsymbol{\chi}}\cdot\boldsymbol{\nabla}B\right)\frac{\partial p_{\text{avg}}}{\partial B} \tag{C9}$$

$$= -\boldsymbol{\kappa}_{\boldsymbol{\chi}}|\boldsymbol{\nabla}\Psi|\frac{\partial p_{\text{avg}}}{\partial\Psi} - \boldsymbol{\kappa}_{\boldsymbol{\chi}}\left(\hat{\boldsymbol{e}}_{\boldsymbol{\Psi}}\cdot\boldsymbol{\nabla}B\right)\frac{\partial p_{\text{avg}}}{\partial B} + \frac{j_\parallel}{B}\left(\hat{\mathbf{b}}\cdot\boldsymbol{\nabla}B\right)\frac{\partial p_{\text{avg}}}{\partial B} + \boldsymbol{\kappa}_{\boldsymbol{\Psi}}\left(\hat{\boldsymbol{e}}_{\boldsymbol{\chi}}\cdot\boldsymbol{\nabla}B\right)\frac{\partial p_{\text{avg}}}{\partial B}, \tag{C10}$$

so that now

$$\delta W_{F+A}^{\text{ballooning}} = \int \left(|\boldsymbol{\xi}_{\boldsymbol{\Psi}}|^2\boldsymbol{\kappa}_{\boldsymbol{\Psi}}\left(|\boldsymbol{\nabla}\Psi|\frac{\partial p_{\text{avg}}}{\partial\Psi} + \hat{\boldsymbol{e}}_{\boldsymbol{\Psi}}\cdot\boldsymbol{\nabla}B\frac{\partial p_{\text{avg}}}{\partial B}\right) + |\boldsymbol{\xi}_{\boldsymbol{\chi}}|^2\boldsymbol{\kappa}_{\boldsymbol{\chi}}\left(\hat{\boldsymbol{e}}_{\boldsymbol{\chi}}\cdot\boldsymbol{\nabla}B\frac{\partial p_{\text{avg}}}{\partial B}\right)\right.$$
$$\left. + \boldsymbol{\xi}_{\boldsymbol{\Psi}}\boldsymbol{\xi}_{\boldsymbol{\chi}}^*\left(\frac{j_\parallel}{B}\left(\hat{\mathbf{b}}\cdot\boldsymbol{\nabla}B\right)\frac{\partial p_{\text{avg}}}{\partial B} - \boldsymbol{\nabla}\times\hat{\mathbf{b}}\cdot\boldsymbol{\nabla}p_{\text{avg}}\right)\right) d\mathbf{V}. \tag{C11}$$

From the equilibrium considered in Sec. III, one can show that the last term can be replaced so that (more detail?)

$$\delta W_{F+A}^{\text{ballooning}} = \int \left(|\boldsymbol{\xi}_{\boldsymbol{\Psi}}|^2\boldsymbol{\kappa}_{\boldsymbol{\Psi}}\left(|\boldsymbol{\nabla}\Psi|\frac{\partial p_{\text{avg}}}{\partial\Psi} + \hat{\boldsymbol{e}}_{\boldsymbol{\Psi}}\cdot\boldsymbol{\nabla}B\frac{\partial p_{\text{avg}}}{\partial B}\right) + |\boldsymbol{\xi}_{\boldsymbol{\chi}}|^2\boldsymbol{\kappa}_{\boldsymbol{\chi}}\left(\hat{\boldsymbol{e}}_{\boldsymbol{\chi}}\cdot\boldsymbol{\nabla}B\frac{\partial p_{\text{avg}}}{\partial B}\right)\right.$$
$$\left. + \boldsymbol{\xi}_{\boldsymbol{\Psi}}\boldsymbol{\xi}_{\boldsymbol{\chi}}^*\mathbf{B}\boldsymbol{\nabla}\cdot\left(\frac{\sigma j_\parallel}{2}\hat{\mathbf{b}}\right)\right) d\mathbf{V}. \tag{C12}$$

Then one can see that

$$\delta W_{F+A}^{\text{kink}} + \delta W_{F+A}^{\text{ballooning}} = \frac{1}{2}\int \left(\frac{\sigma j_\parallel}{2B}\left((\boldsymbol{\xi}_\perp \times \mathbf{B})\cdot\tilde{\mathbf{B}}_\perp^* + (\boldsymbol{\xi}_\perp^* \times \mathbf{B})\cdot\tilde{\mathbf{B}}_\perp\right) + \left(\boldsymbol{\xi}_{\boldsymbol{\Psi}}\boldsymbol{\xi}_{\boldsymbol{\chi}}^* + \boldsymbol{\xi}_{\boldsymbol{\chi}}\boldsymbol{\xi}_{\boldsymbol{\Psi}}^*\right)\mathbf{B}\boldsymbol{\nabla}\cdot\left(\frac{\sigma j_\parallel}{2}\hat{\mathbf{b}}\right)\right. \tag{C13}$$
$$\left. + 2|\boldsymbol{\xi}_{\boldsymbol{\Psi}}|^2\boldsymbol{\kappa}_{\boldsymbol{\Psi}}\left(|\boldsymbol{\nabla}\Psi|\frac{\partial p_{\text{avg}}}{\partial\Psi} + \hat{\boldsymbol{e}}_{\boldsymbol{\Psi}}\cdot\boldsymbol{\nabla}B\frac{\partial p_{\text{avg}}}{\partial B}\right) + 2|\boldsymbol{\xi}_{\boldsymbol{\chi}}|^2\boldsymbol{\kappa}_{\boldsymbol{\chi}}\left(\hat{\boldsymbol{e}}_{\boldsymbol{\chi}}\cdot\boldsymbol{\nabla}B\frac{\partial p_{\text{avg}}}{\partial B}\right)\right) d\mathbf{V},$$

is self-adjoint.

[1] M. S. Chu and M. Okabayashi, Plasma Physics and Controlled Fusion **52**, 123001 (2010).
[2] M. D. Kruskal and C. R. Oberman, The Physics of Fluids **1**, 275 (1958).
[3] M. N. Rosenbluth and N. Rostoker, Physics of Fluids **2**, 23 (1959).
[4] J. B. Taylor and R. Hastie, Physics of Fluids **8**, 323 (1965).
[5] T. Antonsen and Y. Lee, Physics of Fluids **25**, 132 (1982).
[6] G. F. Chew, M. L. Goldberger, and F. E. Low, Proceedings of the Royal Society of London, Series A **236**, 112 (1956).
[7] B. Hu and R. Betti, Physical Review Letters **93**, 105002 (2004).
[8] J. W. Berkery, S. A. Sabbagh, R. Betti, B. Hu, R. E. Bell, S. P. Gerhardt, J. Manickam, and K. Tritz, Physical Review Letters **104**, 035003 (2010).
[9] S. A. Sabbagh, J. W. Berkery, R. E. Bell, J. M. Bialek, S. P. Gerhardt, J. E. Menard, R. Betti, D. A. Gates, B. Hu, O. N. Katsuro-Hopkins, B. P. LeBlanc, F. M. Levinton, J. Manickam, K. Tritz, and H. Yuh, Nuclear Fusion **50**, 025020 (2010).
[10] J. W. Berkery, S. A. Sabbagh, H. Reimerdes, R. Betti, B. Hu, R. E. Bell, S. P. Gerhardt, J. Manickam, and M. Podesta, Physics of Plasmas **17**, 082504 (2010).
[11] M. Ono, S. M. Kaye, Y. K. Peng, G. Barnes, W. Blanchard, M. D. Carter, J. Chrzanowski, L. Dudek, R. Ewig, D. Gates, R. E. Hatcher, T. Jarboe, S. C. Jardin, D. Johnson, R. Kaita, M. Kalish, C. E. Kessel, H. W. Kugel, R. Maingi, R. Majeski, J. Manickam, B. McCormack, J. Menard, D. Mueller, B. A. Nelson, B. E. Nelson, C. Neumeyer, G. Oliaro, F. Paoletti, R. Parsells, E. Perry, N. Pomphrey, S. Ramakrishnan, R. Raman, G. Rewoldt, J. Robinson, A. L. Roquemore, P. Ryan, S. Sabbagh, D. Swain, E. J. Synakowski, M. Viola, M. Williams, and J. R. Wilson, Nuclear Fusion **40**, 557 (2000).
[12] B. Hu, R. Betti, and J. Manickam, Physics of Plasmas **12**, 057301 (2005).
[13] S. Coda, I. Klimanov, S. Albertu, G. Arnoux, P. Blanchard, and A. Fasoli, Plasma Physics and Controlled Fusion **48**, B359 (2006).
[14] G. Z. Hao, Y. Q. Liu, A. K. Wang, H. B. Jiang, G. Lu, H. D. He, and X. M. Qiu, Physics of Plasmas **18**, 032513 (2011).
[15] I. T. Chapman, C. G. Gimblett, M. P. Gryaznevich, T. C. Hender, D. F. Howell, Y. Q. Liu, and S. D. Pinches, Plasma Physics and Controlled Fusion **53**, 065022 (2011).
[16] G. Z. Hao, A. K. Wang, Y. Q. Liu, and X. M. Qiu, Physical Review Letters **107**, 015001 (2011).
[17] J. Graves, I. Chapman, S. Coda, L. Eriksson, and T. Johnson, Physical Review Letters **102**, 065005 (2009).
[18] I. T. Chapman, V. G. Igochine, J. P. Graves, S. D. Pinches, A. Gude, I. Jenkins, M. Maraschek, and G. Tardini, Nuclear Fusion **49**, 035006 (2009).
[19] I. T. Chapman, I. Jenkins, R. V. Budny, J. P. Graves, S. D. Pinches, and S. Saarelma, Plasma Physics and Controlled Fusion **50**, 045006 (2008).
[20] E. R. Salberta, R. Grimm, J. L. Johnson, J. Manickam, and W. M. Tang, Physics of Fluids **30**, 2796 (1987).
[21] R. Iacono, A. Bondeson, F. Troyon, and R. Gruber, Physics of Fluids B **2**, 1794 (1990).
[22] L. Guazzotto, R. Betti, J. Manickam, and S. Kaye, Physics of Plasmas **11**, 604 (2004).
[23] W. A. Cooper, J. P. Graves, S. P. Hirshman, T. Yamaguchi, Y. Narushima, S. Okamura, S. Sakakibara, C. Suzuki, K. Y. Watanabe, H. Yamada, and K. Yamazaki, Nuclear Fusion **46**, 683 (2006).
[24] M. Jucker, J. P. Graves, G. A. Cooper, and W. A. Cooper, Plasma Physics and Controlled Fusion **50**, 065009 (2008).
[25] W. A. Cooper, S. P. Hirshman, P. Merkel, J. P. Graves, J. Kisslinger, H. F. G. Wobig, Y. Narushima, S. Okamura, and K. Y. Watanabe, Computer Physics Communications **180**, 1524 (2009).
[26] M. J. Hole, G. von Nessi, M. Fitzgerald, K. G. McClements, and J. Svensson, Plasma Physics and Controlled Fusion **53**, 074021 (2011).
[27] A. Bondeson and R. Iacono, Physics of Fluids B **1**, 1431 (1989).
[28] W. A. Cooper, J. P. Graves, M. Jucker, and M. Y. Isaev, Physics of Plasmas **13**, 092501 (2006).
[29] T. Antonsen, B. Lane, and J. Ramos, Physics of Fluids **24**, 1465 (1981).
[30] A. J. Cerfon and J. P. Freidberg, Physics of Plasmas **18**, 012505 (2011).
[31] J. W. Van Dam, Journal of the Korean Physical Society **31**, S93 (1997).
[32] R. Betti and J. P. Freidberg, Physics of Fluids B **4**, 1465 (1992).
[33] J. Van Dam, M. Rosenbluth, and Y. Lee, Physics of Fluids **25**, 1349 (1982).
[34] A. Bondeson and M. S. Chu, Physics of Plasmas **3**, 3013 (1996).
[35] R. Betti and J. P. Freidberg, Physics of Fluids B **3**, 538 (1991).
[36] P. J. Fielding and F. A. Haas, Physical Review Letters **41**, 801 (1978).
[37] R. O. Dendy, R. J. Hastie, K. G. McClements, and T. J. Martin, Physics of Plasmas **2**, 1623 (1995).
[38] E. R. Salberta, *A Numerical Study of the Effects of Anisotropic Pressure on Ideal MHD Equilibrium and Stability in Tokamaks*, Ph.D. thesis, Princeton University (1986).
[39] R. Grimm, J. Greene, and J. Johnson, "Methods in computational physics, vol. 16," Chap. Computation of the Magnetohydrodynamic Spectrum in Axisymmetric Toroidal Confinement Systems.
[40] S. Preische, J. Manickam, and J. Johnson, Computer Physics Communications **76**, 318 (1993).
[41] M. Chance, Physics of Plasmas **4**, 2161 (1997).
[42] J. Freidberg, *Ideal Magnetohydrodynamics* (Springer, 1987).
[43] B. Hu, R. Betti, and J. Manickam, Physics of Plasmas **13**, 112505 (2006).
[44] W. A. Cooper, D. B. Nelson, G. Bateman, and T. Kammash, Physical Review Letters **43**, 1325 (1979).
[45] W. A. Cooper, Physics of Fluids **26**, 1830 (1983).
[46] F. Porcelli, Plasma Physics and Controlled Fusion **33**, 1601 (1991).
[47] J. Graves, Physical Review Letters **92**, 185003 (2004).
[48] I. T. Chapman, S. D. Pinches, L. C. Appel, R. J. Hastie, T. C. Hender, S. Saarelma, S. E. Sharapov, I. Voisekhovitch, and J. P. Graves, Physics of Plasmas **14**, 070703 (2007).
[49] Y. Liu, M. S. Chu, W. F. Guo, F. Villone, R. Albanese, G. Ambrosino, M. Baruzzo, T. Bolzonella, I. T. Chapman, A. M. Garofalo, C. G. Gimblett, R. J. Hastie, T. C. Hender, G. L. Jackson, R. J. La Haye, M. J. Lanctot, Y. In, G. Marchiori, M. Okabayashi, R. Paccagnella, M. Furno Palumbo, A. Pironti, H. Reimerdes, G. Rubinacci, A. Soppelsa, E. J. Strait, S. Ventre, and D. Yadykin, Plasma Physics and Controlled Fusion **52**, 104002 (2010).
[50] N. Gorelenkov, H. Berk, and R. Budny, Nuclear Fusion **45**, 226 (2005).

[51]A. Polevoi, H. Shirai, and T. Takizuka, "Benchmarking of the NBI block in ASTRA code versus the OFMC calculations," Tech. Rep. (Japan Atomic Energy Research Institute, 1997).
[52]Y. Liu, Nuclear Fusion **50**, 095008 (2010).
[53]C. Angioni, A. Pochelon, N. Gorelenkov, K. McClements, O. Sauter, R. Budny, P. de Vries, D. Howell, M. Mantsinen, M. Nave, and S. Sharapov, Plasma Physics and Controlled Fusion **44**, 205 (2002).
[54]H. Berk, W. Horton, M. Rosenbluth, and P. Rutherford, Nuclear Fusion **15**, 819 (1975).
[55]M. G. von Hellermann, W. G. F. Core, J. Frieling, L. Horton, R. Konig, W. Mandl, and H. Summers, Plasma Physics and Controlled Fusion **35**, 799 (1993).
[56]I. Gradshteyn and I. Ryzhik, *Table of Integrals, Series, and Products* (Academic Press, 2000).
[57]J. W. Berkery, S. A. Sabbagh, R. Betti, R. E. Bell, S. P. Gerhardt, B. P. LeBlanc, and H. Yuh, Physical Review Letters **106**, 075004 (2011).
[58]Y. S. Park, S. A. Sabbagh, J. W. Berkery, J. M. Bialek, Y. M. Jeon, S. H. Hahn, N. Eidietis, T. E. Evans, S. W. Yoon, J. Ahn, J. Kim, H. L. Yang, K. I. You, Y. S. Bae, J. Chung, M. Kwon, Y. K. Oh, W. Kim, J. Y. Kim, S. G. Lee, H. K. Park, H. Reimerdes, J. Leuer, and M. Walker, Nuclear Fusion **51**, 053001 (2011).
[59]H. Reimerdes, J. W. Berkery, M. J. Lanctot, A. M. Garofalo, J. M. Hanson, Y. In, M. Okabayashi, S. A. Sabbagh, and E. J. Strait, Physical Review Letters **106**, 215002 (2011).
[60]J. W. Berkery, R. Betti, and S. A. Sabbagh, Physics of Plasmas **18**, 072501 (2011).
[61]L. Solov'ev, Zh. Eksp. Teor. Fiz. **53**, 626 (1967).
[62]M. S. Chance, J. M. Greene, R. C. Grimm, J. L. Johnson, J. Manickam, W. Kerner, D. Berger, L. C. Bernard, R. Gruber, and F. Troyon, Journal of Computational Physics **28**, 1 (1978).
[63]Y. Liu, M. S. Chu, I. T. Chapman, and T. C. Hender, Physics of Plasmas **15**, 112503 (2008).
[64]R. V. Budny, M. G. Bell, H. Biglari, M. Bitter, C. E. Bush, C. Z. Cheng, E. D. Fredrickson, B. Grek, K. W. Hill, H. Hsuan, A. C. Janos, D. L. Jassby, D. W. Johnson, L. C. Johnson, B. Leblanc, D. C. McCune, D. R. Mikkelsen, H. K. Park, A. T. Ramsey, S. A. Sabbagh, S. D. Scott, J. F. Schivell, J. D. Strachan, B. C. Stratton, E. J. Synakowski, G. Taylor, M. C. Zarnstorff, and S. J. Zweben, Nuclear Fusion **32**, 429 (1992).
[65]R. Budny, Nuclear Fusion **49**, 085008 (2009).
[66]F. M. Poli, C. E. Kessel, M. S. Chance, S. C. Jardin, and J. Manickam, submitted to Nuclear Fusion (2012).
[67]L. Hau and B. Sonnerup, Geophysical Research Letters **20**, 1763 (1993).
[68]R. Prajapati, G. Soni, and R. Chhajlani, Physics of Plasmas **15**, 062108 (2008).
[69]V. Ilgisonis, Physics of Plasmas **3**, 4577 (1996).
[70]I. Grigorev and V. Pastukhov, Plasma Physics Reports **33** (2007).
[71]D. Gurnett and A.Bhattacharjee, *Introduction to Plasma Physics with Space and Laboratory Applications* (Cambridge University Press, 2005).
[72]P. Snyder, G. Hammett, and W. Dorland, Physics of Plasmas **4**, 3974 (1997).
[73]K. M. Ferrière and N. André, Journal of Geophysical Research **107**, 1349 (2002).
[74]H. Hamabata, Journal of Plasma Physics **30**, 291 (1983).